Journal of Volcanology and Geothermal Research 451 (2024) 108116

Contents lists available at ScienceDirect

Journal of Volcanology and Geothermal Research

journal homepage: www.journals.elsevier.com/journal-of-volcanology-and-geothermal-research

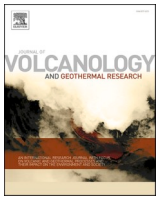

Variable controlling factors lead to contrasting patterns of volcanism in the Changbaishan volcanic area (Tianchi-Longgang), China-North Korea: Insights from morphometry and spatial-temporal analyses

Rong Zhang [a,*], Marco Brenna [a], James D.L. White [a], Gabor Kereszturi [b]

[a] Department of Geology, University of Otago, Dunedin, New Zealand
[b] Volcanic Risk Solutions, School of Agriculture and Environment, Massey University, Private Bag 11 222, Palmerston North, New Zealand

ARTICLE INFO

Keywords:
Changbaishan
Tianchi
Longgang
Monogenetic volcanic field
Volcanism

ABSTRACT

The coexistence of monogenetic and polygenetic volcanoes is a common phenomenon in volcanic areas. However, the genetic relationship between monogenetic and polygenetic systems and the factors controlling their distinct eruptive styles are not well understood. In active volcanic areas, analysing the clustering and vent alignment of monogenetic volcanoes, as well as examining the geomorphology and relative ages of scoria cones, offers quantitative insights into magma supply rates, volcano type distribution, and volcanic development trends. Our study presents geomorphological and spatio-temporal analyses of the *co*-existing monogenetic volcanoes in the Longgang Volcanic Field (LVF) and those associated with a polygenetic volcano (Tianchi) in the Changbaishan Volcanic Area, China. The distance between the two volcanic areas is around 150 km. Monogenetic vents in the LVF exhibit greater density compared to the dispersed system associated with Tianchi. The LVF vents also show better alignment, particularly in the direction of pre-existing basement faults (NE-SW, NW-SE and EW). By using scoria cone morphometric parameters and features, we estimated the relative ages and erupted volumes of monogenetic volcanoes in the LVF and the Tianchi area. We classified the cones of the two volcanic systems into five eruptive periods and found that, despite similar magma sources and output rates over approximately 870 kyr, differing numbers of scoria cones across age classes suggest that Tianchi's magma system influences its associated monogenetic volcanic plumbing. Furthermore, the continuous rise in output rates of monogenetic volcanoes in the Tianchi area highlights the increasing magma supply sustaining Tianchi volcano. Together, these interpretations are consistent with the two systems being controlled by different factors: the Tianchi monogenetic volcanic system is more controlled by magmatism, whereas the LVF is more strongly controlled by local tectonic structures, alongside an increasing magma supply causing the formation of progressively larger individual volcanoes. In volcanic areas, analysing monogenetic volcanoes' spatial-temporal distribution, volumes and recurrence rate provides a framework to evaluate magma supply rates and tectonic associations, which are key to the development of different volcano types.

1. Introduction

Monogenetic volcanic fields are ubiquitous in intraplate settings. They can occur in association with polygenetic volcanoes, either as overlapping systems, such as the Jeju Island Volcanic Field (Brenna et al., 2012, 2015a), or as neighbouring but spatially distinct systems, such as the Auckland Volcanic Field (Kereszturi et al., 2014; Leonard et al., 2017). Monogenetic volcanoes are generally distinguished from polygenetic ones based on eruptive history (monogenetic volcanoes are formed by a single eruption; Wood, 1979), volume (typically $\leq$1 km^3; Németh and Kereszturi, 2015) and morphology (spatter/scoria/tuff cones, tuff rings, maars and lava domes; Connor and Conway, 2000; Kereszturi and Németh, 2012a; Valentine and Connor, 2015; Murcia and Németh, 2020). The differences between monogenetic and polygenetic volcanic systems may be controlled by magma supply rates (Fedotov, 1981; Hildreth, 1981; Takada, 1994; Cañón-Tapia and Walker, 2004), magma extrusive/intrusive ratio (Hildreth, 1981) and/or different tectonic settings (Takada, 1994; Cañón-Tapia and Walker, 2004; Valentine and Perry, 2007). The coexistence of monogenetic and polygenetic volcanoes in a region often involves magmatic and/or tectonic

* Corresponding author.
E-mail address: zrong987114@163.com (R. Zhang).

https://doi.org/10.1016/j.jvolgeores.2024.108116
Received 6 February 2024; Received in revised form 25 May 2024; Accepted 30 May 2024
Available online 31 May 2024

heterogeneity on a local scale (Alaniz-Alvarez et al., 1998; Carn, 2000; Ishizuka et al., 2015). However, despite these advances in understanding, the relationship between monogenetic and polygenetic volcanoes coexisting within the same area, and the mechanisms controlling distinct modes of eruptive activity (dispersed versus centralized) remain unclear.

At the border between China and North Korea, a monogenetic volcanic field (Longgang) and polygenetic volcanoes (Tianchi, Wangtian'e and Namphothe) coexist in the Changbaishan Volcanic Area (CVA) (Lei et al., 2019). The three polygenetic volcanoes are situated next to each other within a 50 km radius, distinct from the monogenetic volcanic field located approximately 150 km away. The Longgang Volcanic Field (LVF) contains approximately 160 monogenetic volcanoes, whereas >200 dispersed vents are distributed on and near the flanks of (within 100 km of), and are interpreted to be associated with, the three polygenetic volcanoes (Zhang et al., 2018; Li et al., 2021). The monogenetic volcanoes in the LVF and those associated with the polygenetic volcanoes have similar eruption ages (peak activity in the Quaternary), tectonic settings, and magma sources (Zhang et al., 2015; Li et al., 2021; Zhao et al., 2021). Magmatism of the polygenetic volcanoes of Changbaishan has generally been attributed to mantle plume activity or passive asthenospheric upwelling driven by settling of the subducted Pacific plate (Zhao et al., 2009; Tang et al., 2014; Kuritani et al., 2019). The more broadly dispersed monogenetic volcanic fields in northeastern China, including the LVF, have likewise been attributed to variable rates of mantle upwelling due to influence from the subducted Pacific plate (Zou et al., 2008). The lithospheric mantle beneath both areas has been metasomatized above the subducted Pacific plate (Xu et al., 2019). All volcanoes also lie on similar lithospheric columns with Moho transitions at depths of ~35–40 km, generally deeper under the polygenetic volcanoes (Zhang et al., 2020). Despite all these similarities, the LVF is a standalone volcanic system. Longgang magma is interpreted to originate from a deeper source region, undergo less differentiation, and rise rapidly to the surface (Zhao et al., 2021). In contrast, monogenetic volcanoes associated with the polygenetic volcanoes might have undergone more complex magmatic evolutions or have been influenced by the polygenetic magmatic system (Li et al., 2021). Analysing the geomorphology and spatio-temporal characteristics of co-existing monogenetic volcanoes in the active LVF, and of those associated with polygenetic volcanoes in the CVA, provide an opportunity to explore the factors controlling different types of volcanism and gain a better understanding of volcanic plumbing systems.

2. Changbaishan Volcanic Area

CVA volcanoes are constructed over a large basaltic platform, i.e., the Gaima lava plateau, developed from ca. 23 to 5 Ma, and located near the northern margin of the Archean-Proterozoic Sino-Korean craton coinciding with the border between China and North Korea (Fig. 1; Wei et al., 2013, Zhang et al., 2018). Active volcanism occurs at the intersection of the NE-trending Tanlu fault system and the NW-trending Paektusan fault system (Andreeva et al., 2014). The volcanoes include

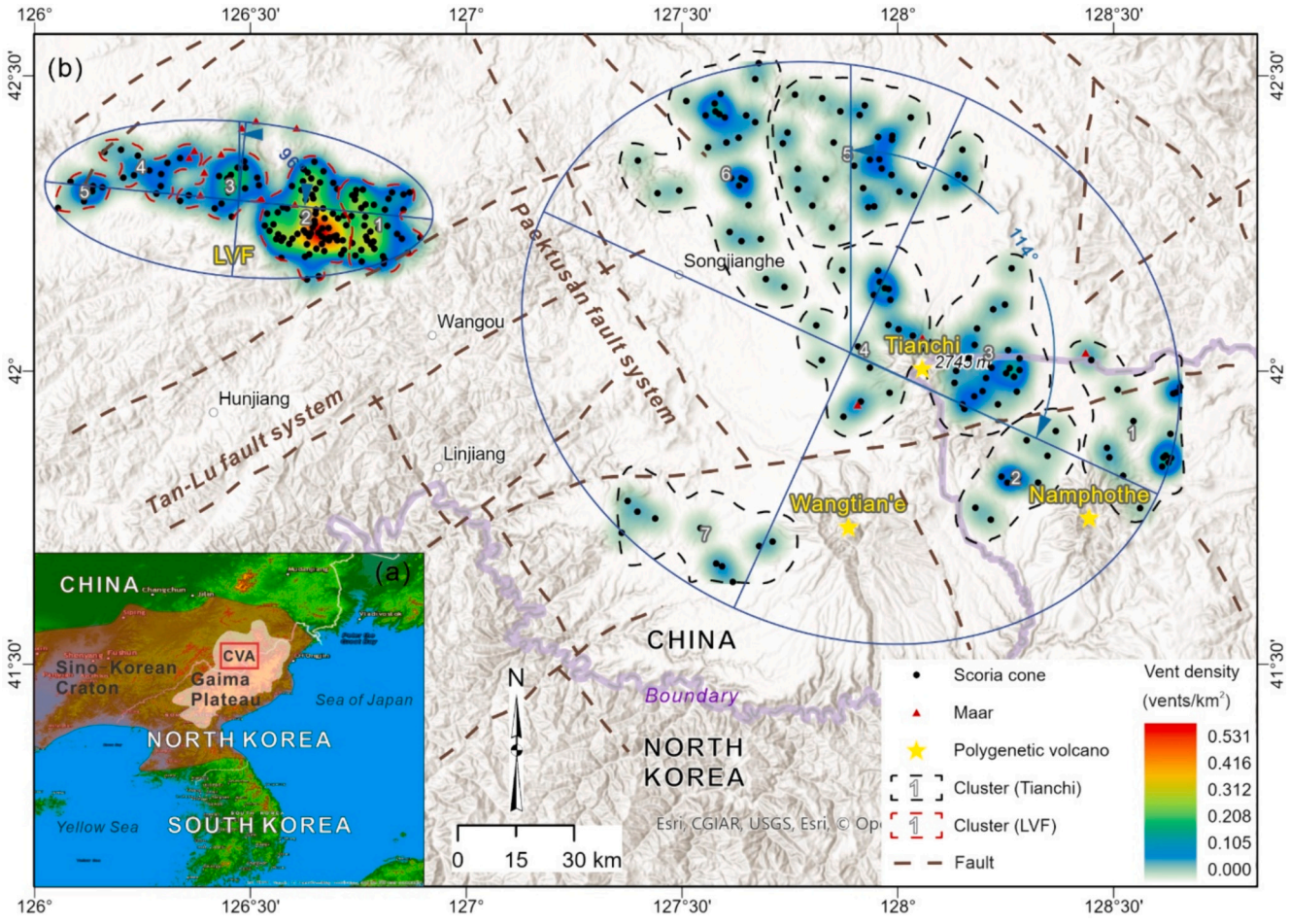

Fig. 1. (a) Location of the Changbaishan Volcanic Area (CVA). Base map from Esri™. (b) Volcanoes in the CVA. Monogenetic volcano clusters defined based on vent density in the Longgang Volcanic Field (LVF) and the Tianchi area, respectively. Calculated minimum ellipses enclosing each volcanic area shown by blue lines. Blue numbers indicate the azimuths of the long axes of the ellipses. Shaded relief base map from Esri™. (For interpretation of the references to colour in this figure legend, the reader is referred to the web version of this article.)

Tianchi on the China-North Korean border, Wangtian'e in NE China, and Namphothe in North Korea, as well as the LVF in China (Fig. 1). They cover an area of about 20,000 km^2. Eruptions have occurred repeatedly from the Pliocene to modern times. The total eruptive volume of the CVA, excluding the LVF, is in the range 1.7 × 10^3 to 5.8 × 10^3 km^3 (Zhang et al., 2018).

2.1. Polygenetic volcanoes and associated monogenetic volcanoes

Tianchi (2745 m above sea level) is a well-preserved Late Cenozoic polygenetic central volcano, and the largest active volcano in China (Wei et al., 1999). During the Holocene, at least one large-scale eruption and several medium to small-scale explosive eruptions have occurred at Tianchi. The "Millennium eruption" of Tianchi with a Volcanic Explosivity Index (VEI) of six has been described as one of the largest eruptions in the world in the last 2000 years (Liu et al., 1997; Yang et al., 2021). In general, Tianchi has undergone growth and evolution progressing from an early shield stage (5.02–1.05 Ma), to a middle cone stage (1.37–0.01 Ma) and a late caldera-forming stage (0.01 Ma to 1903 CE) (Zhang et al., 2018). The eruptive products of the shield period were alkaline and tholeiitic basalt; those of the cone period were trachyte and comendite lava, along with pyroclastic rocks; and the recent eruptive products are mainly comenditic pyroclastic rocks (Wei and Yang, 1998; Wei et al., 1998a, 1998b; Wang et al., 2003; Wei et al., 2013). Wangtian'e is located ca. 35 km southwest of Tianchi (Fig. 1) and consists of a basalt-trachybasalt shield-like plateau (4.77–1.86 Ma) and a trachyandesite-trachyte-rhyolite cone (3.14–2.12 Ma) (Zhang et al., 2018). Based on limited age data, it is suggested that Namphothe, located ca. 45 km southeast of Tianchi, had a basalt-basaltic trachyandesite shield-forming stage (1.22–1.18 Ma) and a trachyandesite-trachyte-rhyolite cone-forming stage (1.79–0.70 Ma) (Zhang et al., 2018).

Over 200 monogenetic volcanoes, including scoria cones and maars, are dispersed through the area surrounding the polygenetic volcanoes (especially Tianchi volcano), with some closely associated with the flanks of the polygenetic volcanoes (Fig. 1) (Jin and Zhang, 1994; Li et al., 2021; Sun et al., 2021). The eruptive products of these monogenetic volcanoes are considered contemporaneous with the construction of Tianchi's cone (ca. 1–0.01 Ma) (Zhang et al., 2018; Lei et al., 2019; Li et al., 2021). They have similar petrological and mineralogical characteristics to the shield-forming lava flows of Tianchi volcano, suggesting they originate from the same mantle source (Chen et al., 2017). In addition, they are believed to be directly derived from the mantle magmatic system that also supports the crustal magmatic system underlying Tianchi volcano (Fan et al., 2006; Chen et al., 2017). Therefore, these monogenetic volcanoes are genetically related to the Tianchi volcano magmatic system, but their overall distance (up to 100 km) precludes their direct derivation from the centralized plumbing and caldera-forming magma reservoirs. The monogenetic volcanoes are classified into two periods: the Laofangzixiaoshan Period (0.87–0.54 Ma), with alkaline basaltic compositions, and the Laohudong Period (0.34–0.1 Ma), which includes both alkaline and tholeiitic basaltic rocks (Qian et al., 2016).

2.2. Longgang Volcanic Field

The LVF is located about 150 km northwest of Tianchi in the central Longgang mountains region (Fig. 1). It is about 70 km long from east to west and about 40 km wide from north to south, and covers an area of >1500 km^2. The Pre-Cenozoic basement in the region comprises mainly Archean metamorphic rocks (Bai et al., 2006). The Quaternary volcanic activity in Longgang has created the modern, cone-dominated topography of the Longgang volcanoes (Fan et al., 2002). Volcanic activity periods were divided into the Xiaoyizishan Period (2.15–0.75 Ma), marked by fissure-type eruptions; the Longgang Period (0.68–0.05 Ma), characterised by explosive eruptions; and the Jinlongdingzi Period (1600-1500a. BP), a more recent phase (Fan et al., 2002). The volcanic field is considered one of the few volcanically active areas in modern China (Liu, 1988; Liu, 2000).

The LVF contains >160 distributed monogenetic volcanoes (Ou and Fu, 1984; Fan and Hooper, 1991; Xie et al., 1993; Liu, 1999; Sui et al., 1999; Fan et al., 2002). Their volcanic eruption styles and volcanic structures are complex and characterised by multi-cycle and multi-stage eruptions forming principally scoria cones and associated lavas, as well as several maars (Bai et al., 2006). Liu (1990) suggested that the LVF volcanoes have obvious directional arrangement, which is controlled by the checkerboard crustal structure dominated by EW-, NE- and NW-trending faults. The EW-striking fault zone is compressional and controls the overall distribution of the volcanoes within the field and hence the orientation of the field. The NE- and NW-striking faults are transcurrent, determining the local distribution of the volcanoes (Zhao et al., 2021; Zhang et al., 2023). The Quaternary volcanic rocks in the LVF are mostly trachybasaltic with abundant ultramafic xenoliths (Sui et al., 1999; Fan et al., 2000; Liu et al., 2009; Yu et al., 2005) and are closer in composition to the primitive mantle and show more primitive geochemical characteristics compared to those surrounding Tianchi (Zhao et al., 2021).

3. Database and methods

3.1. Database

This study used freely available Advanced Land Observing Satellite (ALOS) World 3D 30 m (AW3D30) data, terrain maps (e.g., from Esri, USGS, CGIAR) and satellite images (e.g., from Maxar). AW3D30 is a free 30 m spatial resolution digital elevation model (DEM) with near complete global coverage. It has a target accuracy of 5 m (root mean square error) and was determined to be the most accurate freely available global DEM for monogenetic volcano applications (Takaku et al., 2014; Zhang et al., 2022). Based on these data, we manually located 150 monogenetic volcanoes in the LVF area, comprising of 140 scoria cones and 10 maars, and 137 monogenetic volcanoes in the Tianchi area, consisting of 134 scoria cones and 3 maars. According to Zhang et al. (2022), the computation of morphometric parameters (volume, slope, height) of scoria cones using the AW3D30 gives errors of ≤15.7% for cones with volumes <5 × 10^6 m^3, and errors of ≤10% for cones with volumes ≥5 × 10^6 m^3. In this study, there are 99 scoria cones with volumes <5 × 10^6 m^3 and an additional 175 with volumes ≥5 × 10^6 m^3 (refer to Supplementary Data 1).

3.2. Spatial analysis

Analysis of the spatial distribution of monogenetic volcanoes allows detailed studies of local tectonic conditions and vent density (Le Corvec et al., 2013; Schmidt et al., 2022), as well as conditions that may favour the formation of large volcanoes. The CVA is ideal for this because of the large number and good preservation of monogenetic volcanoes.

3.2.1. Cluster analysis

To discuss trends in the spatial development of volcanic fields, we performed a cluster analysis of monogenetic volcanoes in the LVF and the Tianchi area. The Kernel Density tool of ArcGIS Pro was used to prepare vent density maps (c.f. van den Hove et al., 2017), which might not directly correspond to event/eruption density maps (Runge et al., 2014). A search radius of 5 km was used, which is close to 2–3 times the mean vent separation in both volcanic areas. This search radius reflects the local scale range of the volcano distribution density in both volcanic areas (Mazzarini, 2007). The monogenetic volcanoes in the Tianchi area were manually grouped into 7 clusters, while those in the LVF were manually divided into 5 clusters (see Fig. 1 and Supplementary Data 1).

3.2.2. Vent alignment analysis

Vent alignment analysis can reveal the potential paths of magma rising to the surface and reflect the controlling tectonic/structural factors (Le Corvec et al., 2013). We used the MATLAB tool of Thomson and Lang (2016) to determine vent alignments. The tool was designed based on the two-point azimuth method of Lutz (1986) and the modified two-point azimuth method of Cebriá et al. (2011). The alignments of all pairs of features are determined by the method of Lutz (1986), with preferred alignments illustrated by peaks in a histogram. The Lutz (1986) method is, however, area sensitive (Cebriá et al., 2011). To eliminate this influence, the raw histogram is normalized by Monte Carlo simulations of random patterns with the same number of points and similar spatial extent. Consequently, a 95% confidence level is calculated to determine significant peaks. In the method of Cebriá et al. (2011), azimuths are only calculated between features within the minimum significant distance, $d_{ms} = |x - 1\sigma|/3$, where x is the mean separation distance and σ is the standard deviation.

3.2.3. Poisson nearest neighbour analysis

Poisson Nearest Neighbour (PNN) analysis can statistically characterize the distribution of vents in monogenetic volcanic areas to quantify the degree of clustering and the spatial correlation between volcanoes. This is based on the comparison of the mean nearest neighbour (NN) distance of an observed population (R_o) with the mean NN distance calculated from an idealised Poisson distribution (R_e) (Le Corvec et al., 2013; Paguican et al., 2021). A convex hull is employed to define the volcanic area for the population density estimation (Le Corvec et al., 2013). The ratio (R) is equal to R_o/R_e. The c statistical test is used to assess the quality of the fit with the Poisson distribution (Clark and Evans, 1954). A Poisson distribution will ideally show 1 for R value and 0 for c value. Values of R greater than and less than 1 mean that the distribution of the population is more dispersed and clustered than the Poisson distribution, respectively (Beggan and Hamilton, 2010). We used the MATLAB-based Geological Image Analysis Software (GIAS) (Beggan and Hamilton, 2010) for the PNN analysis. Since the R and c statistical values are based on the population size, the values are plotted with a confidence interval of 2σ to overcome the sample-dependent bias and assess the fitness of the PNN analysis (Beggan and Hamilton, 2010).

3.2.4. Shape of monogenetic volcanic fields

The shape of a volcanic field can provide important information about where magma is generated and its behaviour from source to surface (Condit and Connor, 1996; Le Corvec et al., 2013; Paguican et al., 2021). Shapes are determined by various factors, including magma generation processes and tectonic environment (Le Corvec et al., 2013). We used the function getMinEllipse of the package 'shotGroups' in the R software (Wollschlaeger, 2022) to define the minimum enclosing ellipses of the LVF and the Tianchi area.

3.3. Morphometric analysis of scoria cones

Most of the scoria cones in the CVA are horseshoe-shaped with one or two craters, some are intact cones with a crater, and a few are cones without craters. The outlines of scoria cone base and crater were manually delimited following slope breaks around their base and crater edges. For analysing the crater and cone diameters, the crater and base of breached cones were manually reconstituted to circular shapes (Fig. 2a), while all other morphometric parameters were calculated based on the outlines of the scoriaceous deposits (Fig. 2b).

We used ArcGIS Pro to estimate the planimetric areas of scoria cone base (Aco) and crater (Acr). Following Favalli et al. (2009), average diameters of the cone base (Wco) and crater (Wcr) were defined as:

$$Wco = 2\sqrt{Aco/\pi} \quad (1)$$

$$Wcr = 2\sqrt{Acr/\pi} \quad (2)$$

The volume of each scoria cone was estimated from the space enclosed by the current surface and the pre-eruption surface, modelled by the interpolation of a triangulated irregular network (TIN) function (c.f., Kereszturi et al., 2013b). The erupted volume of a scoria cone is defined as:

$$Vco = \sum \Delta z_i xy \quad (3)$$

where Δz_i is the elevation difference between the current and the pre-eruptive surface at the grid cell i, and x and y are the dimensions of the pixel size along the two main principal directions.

The maximum height of scoria cones (Hco) was quantified following Favalli et al. (2009), as:

$$Hco = \Delta z_{max} \quad (4)$$

where Δz_{max} is the maximum elevation difference between the crater rim and the pre-eruption surface.

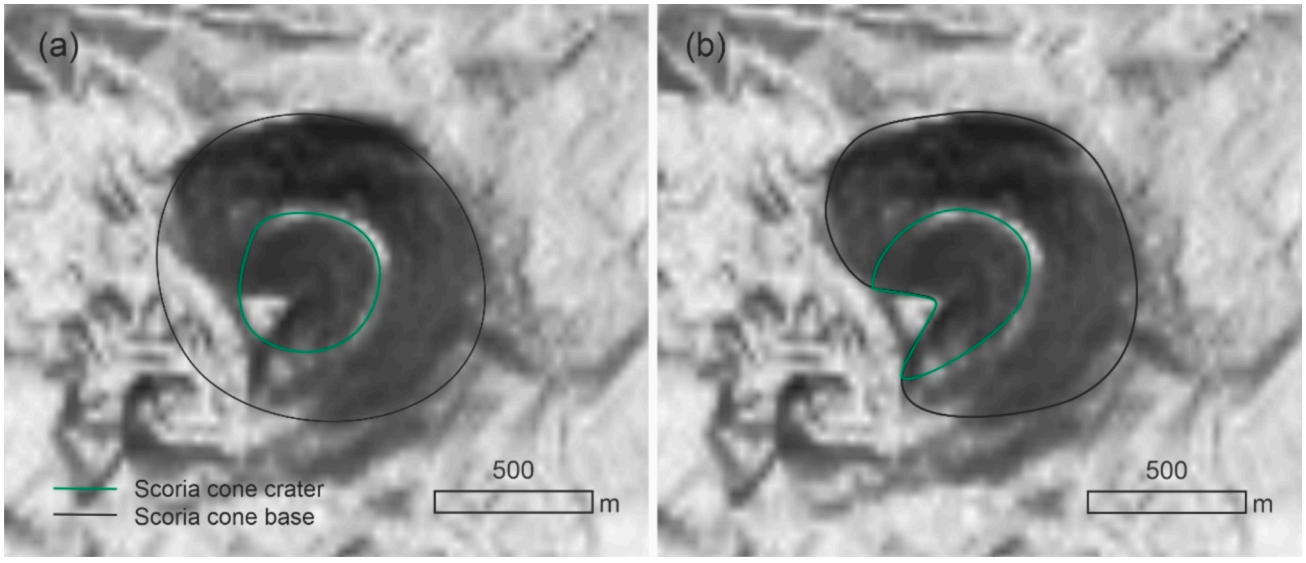

Fig. 2. Definition of the base and crater of a breached scoria cone (No. 240). (a) Reconstituted cone base and crater. (b) Delineated cone base and crater. Shaded relief base map from AW3D30.

The maximum crater depth (*Dcr*) was calculated by subtracting the minimum elevation from the maximum elevation of the crater.

The mean outer flank slope angle of the scoria cone (*Sco-f*), the mean slope angle of the pre-eruption basement (*Sba*) and the mean inner slope angle of the crater (*Scr*) were calculated for each scoria cone. The ratios *Hco/Wco*, flat-topped-ness (*Wcr/Wco*), steep-sided-ness (*2Hco/(Wco-Wcr)*), and *Dcr/Wcr* were also estimated for each scoria cone. Detailed information of morphometric parameters of scoria cones in the LVF and the Tianchi area are reported in Supplementary Data 1.

According to Zhang et al. (2023), *Wco* is the best indicator of the volume of lava flows related to individual scoria cones. The volume of the lava flow associated with a scoria cone is defined as:

$$Vla = 10.32e^{0.003Wco} \quad (5)$$

When the proportion of scoria cones surpasses 90% of the total number of vents within a volcanic field, the planimetric scoria cone output rate becomes a dependable parameter for assessing the magma flux rate. This method involves calculating the total base area of all scoria cones to represent the total eruptive volume of a volcanic field (Zhang et al., 2023). Additionally, the volume of volcanic eruptions is estimated by summing the volumes of the scoria cones and their associated lava flows. To minimize the impact of lava breaches and/or degradation on the cone volumes, the method of Riedel et al. (2003) is used to estimate their ideal volume.

3.4. Relative age of scoria cones

To compare the spatial and temporal evolution of monogenetic volcanoes in the LVF and the Tianchi area, we conducted relative age analysis using cone morphology. Morphological parameters of scoria cones, such as *Dcr*, *Dcr/Wcr*, *Scr*, *Sco-f*, *Hco*, and *Hco/Wco* can provide first-order information on relative age, with decreasing values with age (Hooper and Sheridan, 1998; Fornaciai et al., 2012; Kereszturi and Németh, 2012b; Kereszturi et al., 2013a; Grosse et al., 2020). In this study, scoria cones were categorized as intact, breached, and mound-like. Furthermore, based on the number of craters, they were classified into three types: single crater, multiple craters, and craterless (Supplementary Data 1). For analysing the relative ages of intact scoria cones with a crater, four morphometric parameters *Dcr*, *Scr*, *Dcr/Wcr*, and *Hco* were taken into account (Table 1). However, for the breached scoria cones, only *Scr* and *Hco* were considered, as the breaching changes the crater depth (Bemis and Ferencz, 2017). Furthermore, for more complex breached scoria cones with multiple craters, only *Scr* was considered (Table 1) because volcanic materials ejected from two craters may disperse laterally, thereby reducing *Hco*. Lastly, for the analysis of scoria cones without a crater (i.e., "scoria mounds"), only *Hco* was considered. Scoria cones with absolute age data can be used to calibrate relative age classes and provide reference for the geomorphological characteristics of scoria cones. Seven scoria cones from the LVF have absolute age data, of which five are K—Ar ages (110 ka, 240 ka, 270 ka, 620 ka and 680 ka) (Fan et al., 2002), one is a U-series component age (71 ka) (Yu et al., 2005), and another is a ^{14}C age from a volcanic tephra layer (1.59 ka) (Liu et al., 1989). Three scoria cones from the Tianchi area have K—Ar ages (340 ka, 750 ka and 870 ka) (Qian et al., 2016). Based on the division of volcanic activity periods in the two volcanic areas (see Section 2), we grouped the scoria cones into five classes following Haag et al. (2019): (1) ancient (>870 ka), (2) old (870–540 ka), (3) mature (540–340 ka), (4) moderately mature (340–100 ka), and (5) young (≤100 ka). The age grouping comprehensively considers absolute age, relative age derived from geomorphological parameters, and age classes represented by geomorphological features (Fig. 3).

Table 1
Geomorphological parameters for analysing scoria cone relative age based on different types of scoria cones.

Cone type	Crater type	Cone number		Scr	Dcr	Hco	Dcr/Wcr
		LVF	Tianchi				
Intact	One crater	4	10	√	√	√	√
Breached	One crater	122	103	√		√	
	Two craters	6	1	√			
Mound-like	No crater	8	20			√	

4. Results

4.1. Spatial distribution

The kernel density map (Fig. 1) reveals that the density of monogenetic volcanoes in the LVF is substantially higher than that in the Tianchi area. In the LVF, from east to west, the density gradually decreases from clusters 1 and 2 (about 0.531–0.312 vents/km^2) to clusters 4–5 (about 0.105 vents/km^2). The density distribution of clusters in the Tianchi area is <0.105 vents/km^2, and there are no particularly high- or low-density areas (Fig. 1). The overall density of the LVF is 0.107 vents/km^2, whereas that of the Tianchi area is 0.017 vents/km^2 (Table 2).

The PNN analysis indicates that both the LVF and the Tianchi area have c-statistic values $<-2\sigma$ and R-statistic values $<-2\sigma$, indicating that their vent distributions are clustered relative to the Poisson distribution (Table 2). The Tianchi area shows a lower R-statistic value than the LVF, indicating that monogenetic volcanoes in the Tianchi area are more clustered than in the LVF (Table 2).

The LVF shows a more elongate volcanic area shape than the Tianchi area, with the minimum ellipse short axis/long axis value of 0.38 for the LVF versus 0.81 for the Tianchi area (Table 2). The long axis azimuth of the minimum ellipse of the LVF is about 96° and that of the Tianchi area is approximately 114° (Fig. 1 and Table 2), suggesting that their distribution is likely controlled by different factors.

In analysing vent alignment in the LVF, one direction (WNW-ESE) was derived from the method of Lutz (1986) (Table 2 and Fig. 4a). However, the Cebriá et al. (2011) method shows possible vent alignments in the NE-SW, NW-SE and EW directions, in agreement with findings from Zhao et al. (2021), indicating potential faulting controls on the spatial vent distribution (Table 2 and Fig. 4b). In contrast, the Tianchi area has only one significant volcanic alignment direction (NW-SE) derived from the Lutz (1986) method and coinciding with the trend of a fault set, while the NNE-SSW direction determined by the Cebriá et al. (2011) method does not overlap with any fault system (Table 2 and Fig. 4c-d).

4.2. Morphometry of scoria cones

Cone diameter (Wco) and crater diameter (Wcr) in the Tianchi area show a gradual overall increase away from Tianchi volcano, with notable decreases in clusters 1 and 4, while Wcr and Wco increase from east to west in the LVF (Fig. 5a-b). In contrast, cone height (Hco) and volume (Vco) in the centre of the LVF are higher compared to its margins, while these parameters change minimally in the Tianchi area (Fig. 5c-d). Wco is considered to be the parameter least affected by later onlapping lava flows (Zhang et al., 2023). The distribution patterns of Hco and Vco in the LVF show significant differences from Wco, which may be due to lava flow burial of the base of scoria cones, leading to an underestimation of these parameters, especially in LVF cluster 5.

Morphological parameters such as Scr, Dcr, Dcr/Wcr and Sco-f are sensitive to degradation and show similar variation trends among the clusters (Fig. 5e-h). In the Tianchi area, clusters 2, 6 and 7 have lower mean values for these parameters, while the values for the other Tianchi clusters are close to, but lower than, those of the LVF clusters except cluster 5. The highest values for clusters 3 and 4 in the LVF (Fig. 5e-h) agree with these clusters containing the youngest monogenetic volcanoes (Jinglongdingzi and Dayizishan) in the CVA (Liu et al., 1989; Yu et al., 2005). Most of the scoria cones in both volcanic areas formed on pre-eruptive terrain with ≤5° slope (Sba; Fig. 5i), thus their slope angle

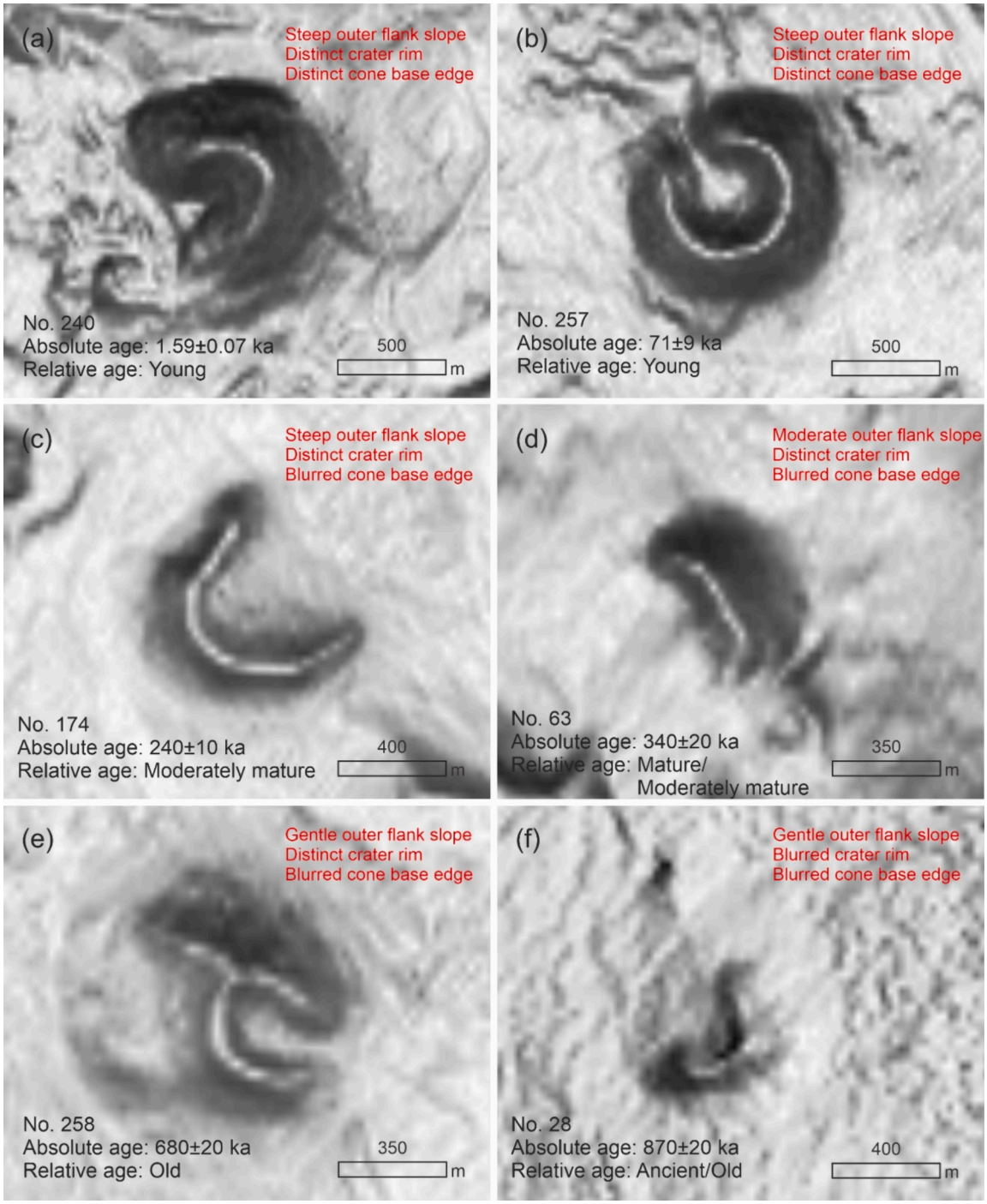

Fig. 3. Geomorphological characteristics of different volcanic age classes. (a-b) Young. (c) Moderately mature. (d) Mature/Moderately mature. (e) Old. (f) Ancient/Old. Shaded relief base map from AW3D30.

variations can be assumed to be minimally affected by the pre-eruptive terrain (Kereszturi et al., 2012).

The scoria cones in the LVF exhibit slightly higher flat-topped-ness values (Wcr/Wco) in comparison to the Tianchi scoria cones (Fig. 6a-b). This difference could be related to climatic/altitude differences and potential phases of phreatomagmatic eruptions (Fornaciai et al., 2012; Aguilera et al., 2022). The average altitude of the scoria cones in the two volcanic areas differs by about 400 m (see Supplementary Data 1). Furthermore, hydrovolcanic activity is an important characteristic of the LVF, resulting in at least 10 maar volcanoes, while only 3 maars are known in the Tianchi area (Ou and Fu, 1984; Jin and Zhang, 1994; Liu et al., 2009; Sun et al., 2021; Zhao et al., 2022). At a given Wco, the scoria cone Wcr and Dcr values of the LVF are greater than those of the Tianchi area (Fig. 6d-e), which may be related to phreatomagmatic eruptions which tend to produce relatively larger craters (Aguilera et al., 2022). Even though there are local variations, the distributions of Hco and Scr vs. Wco in the two areas are remarkably similar (Fig. 6c and f).

4.3. Relative ages of scoria cones

X-Y scatter plots between the absolute ages of the seven dated scoria cones of the LVF and their morphometric parameters show a logarithmic

Table 2
Properties and results of spatial analysis for monogenetic volcanoes in the LVF and the Tianchi area.

	Monogenetic volcanic area	LVF	Tianchi
Measured NN properties	Number of vents	150	137
	Number of vents in convex hull	140	126
	Area convex hull (km^2)	1310	7442
	Density (vents/km^2)	0.107	0.017
	Min NN distance (m)	543	542
	Max NN distance (m)	6287	7340
	Mean NN distance (m)	1440	2771
	Standard deviation (2σ) (m)	1649	3313
	Skewness	2.39	0.96
	Kurtosis	9.38	0.35
NN results relative to the Poisson model	Poisson expected mean NN distance (m)	1532	3843
	R	0.94	0.72
	R positive thresholds at 2σ	1.13	1.14
	R negative thresholds at 2σ	0.94	0.94
	Distribution implication	Clustered	Clustered
	c	−1.36	−5.99
	c positive thresholds at 2σ	3.03	3.04
	c negative thresholds at 2σ	−1.34	−1.35
Alignment analysis	Lutz (1986) method	WNW-ESE	NW-SE
	Cebriá et al. (2011) method		NNE-SSW
	Zhao et al. (2021) inferred	NE-SW, NW-SE, EW	
Shape analysis (minimum ellipse)	Short axis (m)	19	70
	Long axis (m)	50	86
	Short axis/Long axis	0.38	0.81
	Azimuth of long axis	96°	114°

correlation with age for Scr, Dcr/Wcr, Dr. and Hco ($R^2 \geq 0.74$) (Fig. 7a-d). However, Hco/Wco and Sco-f show scattered patterns (Fig. 7e-f). Although there are only three absolute ages of scoria cones in the Tianchi area, they also show a similar trend to the LVF scoria cones (Fig. 7). Furthermore, the logarithmic trend lines of the overall data are consistent with those of the individual volcanic areas, showing that the correlation coefficients (R^2) of Scr, Dcr/Wcr, Dcr and Hco with absolute age are >0.62 (Fig. 7a-d).

To compare the spatio-temporal distribution of scoria cones in the LVF and the Tianchi area, we morphometrically classified all scoria cones into age groups using parameters in Tables 1 and 3 as well as geomorphological features.

In the ancient group, the number of cones in the LVF is twice that of the Tianchi area. Due to the lack of convincing absolute age data, the reasons for this disparity are not discussed here. In the LVF, the number of scoria cones remains consistent across age classes (old to young), while in the Tianchi area, there are progressively fewer young cones (Fig. 8). Furthermore, in the LVF, the ancient and old groups are concentrated in clusters 1, 2, and 3, while the mature and moderately mature groups are focused in cluster 2, and the young group in clusters 2, 3, 4, and 5 (Fig. 8). This can indicate the temporal progression of volcanism and the evolution of the Longgang volcano from east to west. However, in the Tianchi area, the distribution across each group is relatively even (Fig. 8).

5. Discussion

5.1. Scoria cones morphology

Many studies (e.g., Wood, 1980; Hooper and Sheridan, 1998; Guilbaud et al., 2012; Kereszturi et al., 2013a; Haag et al., 2019) have used steepness parameters of scoria cones, e.g., Hco/Wco and Sco-f, to derive the relative age of cones, which is based on the assumption that the original cones have similar morphological parameters, e.g., Hco/Wco =

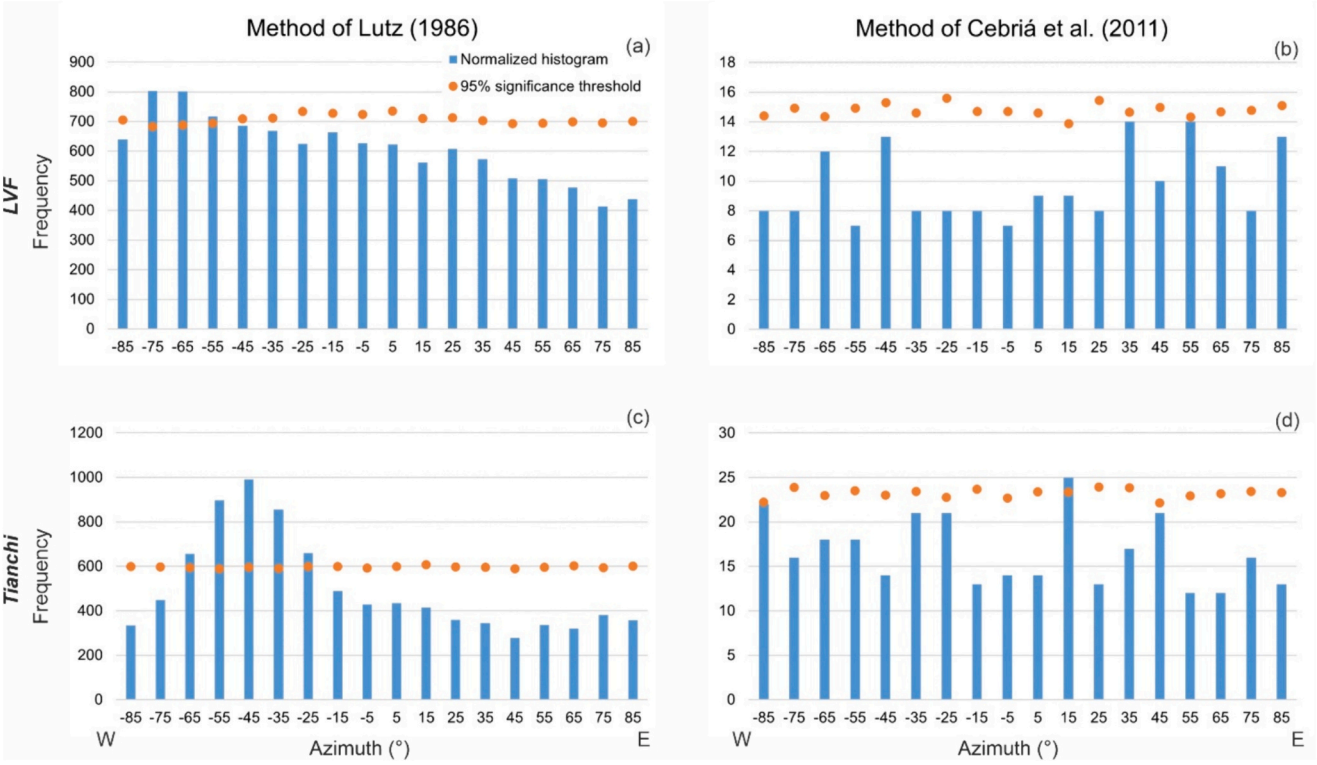

Fig. 4. Histograms of vent alignments of monogenetic volcanoes in the LVF and the Tianchi area with (a) and (c) the two-point azimuth method of Lutz (1986) and (b) and (d) the simplified two-point azimuth method of Cebriá et al. (2011). 100 Monte Carlo models were run for each analysis.

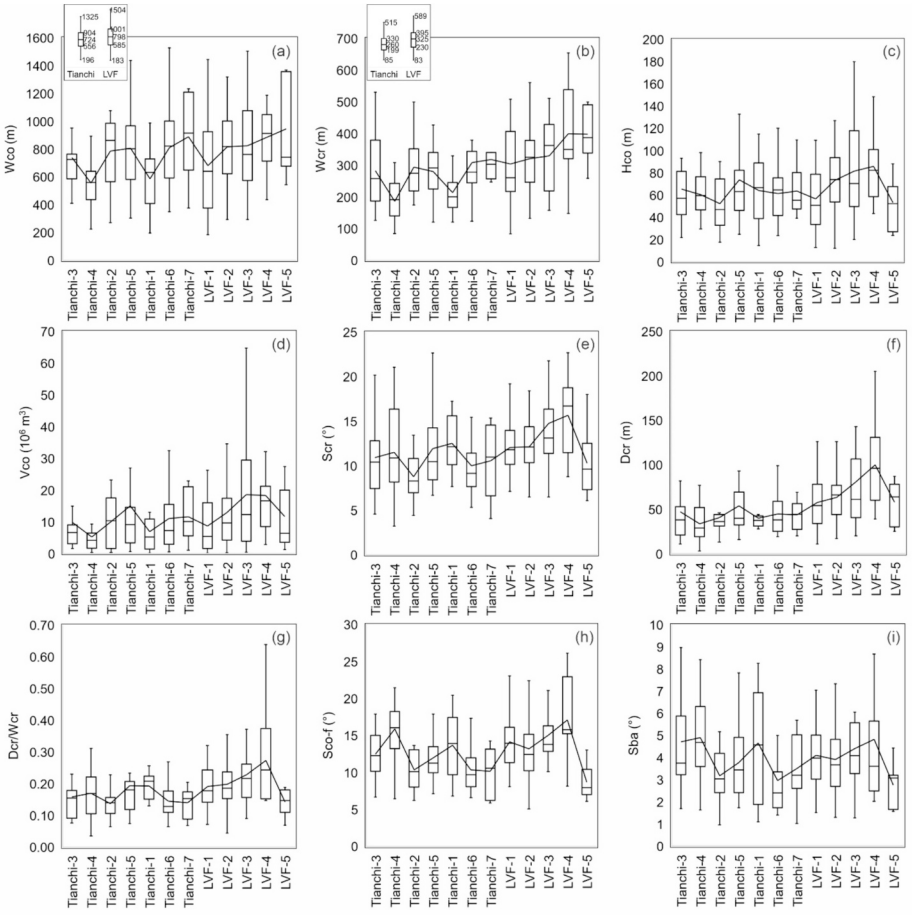

Fig. 5. Boxplots of morphometric parameters (a) Wco, (b) Wcr, (c) Hco, (d) Vco, (e) Scr, (f) Dcr, (g) Dcr/Wcr, (h) Sco-f and (i) Sba for scoria cones in the LVF and around Tianchi, classified according to clusters in Fig. 1. The clusters on the x-axis from left to right are from closest to farthest to Tianchi volcano (see Supplementary Data 1). Black lines show mean values. Insets in (a) and (b) are the overall distributions of Wco and Wcr for the Tianchi area and the LVF, respectively. Wco = Cone base width, Wcr = Crater width, Hco = Cone height, Vco = Cone volume, Scr = Mean inner slope of crater, Dcr = Crater depth, Sco-f = Mean flank slope of cone, and Sba = Mean slope of pre-eruption basement.

0.18, Wcr/Wco = 0.4, Sco-f = 33° (Porter, 1972; Wood, 1980), degradation processes and pyroclastic deposits. However, volcanic systems can often have different characteristics reflecting the local environment, magma composition, eruption type and other factors (e.g., Riedel et al., 2003; Martin and Németh, 2006; Favalli et al., 2009; Bemis et al., 2011; Kervyn et al., 2012; Cimarelli et al., 2013; Kereszturi et al., 2013a; Bemis and Ferencz, 2017). We found that the morphometric parameters that are best correlated with age are the crater-related parameters as well as Hco in the CVA, which is consistent with Grosse et al. (2020). These authors reported that in the Peinado and Incahuasi volcanic fields, southernmost Central Volcanic Zone of the Andes, Dcr, Dcr/Wcr, Dcr/Hco, Scr vs. age have better correlations ($R^2 \geq 0.68$) compared to other morphometric parameters. This may indicate that the outer slope characteristics of the scoria cones in the CVA area are variable due to extrinsic or intrinsic factors, such as local climate, vegetation, magma composition, among others, whereas the crater parameters are less affected. Therefore, using morphometric parameters of scoria cones for relative age analysis should be carefully considered on a case-by-case basis. This is seen also in the different correlations we found for the LVF and Tianchi scoria cone populations (Fig. 7).

5.2. Spatial-temporal distribution and controlling factors

Two distinct monogenetic volcanic systems have developed in the CVA: the standalone LVF and the Tianchi monogenetic field associated with Tianchi composite volcano. They show remarkable differences in the mean NN distance (1440 vs. 2771 m; Table 2) and vent density (0.107 vs. 0.017 vents/km^2; Table 2). These vent densities are in agreement with those calculated for similar volcanic fields (Le Corvec et al., 2013). Compared with a Poisson distribution, the vents in both volcanic areas are clustered, suggesting that systematic nonrandom processes, such as magmatic and tectonic activities, govern vent distribution (Bruno et al., 2006; Le Corvec et al., 2013). A higher magma rejuvenation rate and flux rate can repeatedly generate more clustered volcanic fields (Valentine and Connor, 2015). In the LVF, the planimetric scoria cone output rate is 0.072 km^2/kyr during the last 870 ka, equating to a volumetric volcanic output rate of 0.027 km^3/kyr, following Zhang et al. (2023). Similarly, in the Tianchi area, the planimetric scoria cone output rate is 0.064 km^2/kyr during the last 870 ka, corresponding to a volumetric volcanic output rate of 0.023 km^3/kyr (Table 4). Similar magma flux but different patterns of vent number development in the two volcanic fields (Fig. 8) may be related to the influence of the magma plumbing system of the Tianchi volcano. Tianchi volcano is considered to have a two-layer magma system in which mantle-derived potassic trachybasalt magma feeds eruptions on the surface, forming scoria cones (Fan et al., 2006). The rates of magma generation and supply into the plumbing system have varied over time (e.g., Kuritani et al., 2009), likely associated with complexities in the tectonic drivers of magmatism (e.g., Kimura et al., 2018). However, when a continuous supply is available, the crustal magma chamber feeds more evolved eruptions with abundant fractional crystallization and mixing (Fan et al., 2007a). Therefore, with an increasing magma supply,

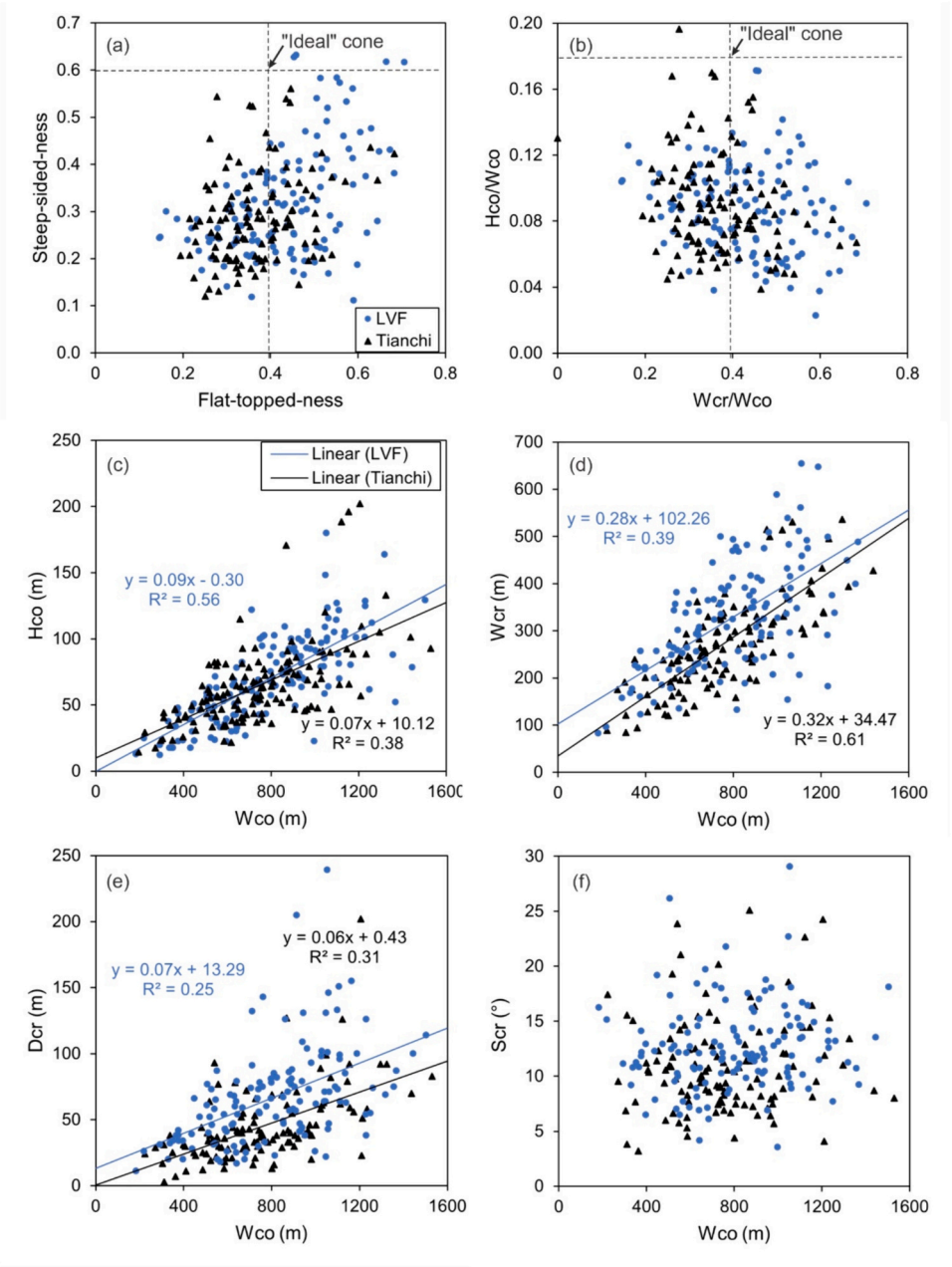

Fig. 6. X-Y plots of morphometric parameters for scoria cones in the LVF and the Tianchi area. (a) Flat-topped-ness vs. steep-sided-ness. (b) Wcr/Wco vs. Hco/Wco. (c) Wco vs. Hco. (d) Wco vs. Wcr. (e) Wco vs. Dcr. (f) Wco vs. Scr. The "ideal" cone values are from Porter (1972) and Wood (1980). Wco = Cone base width, Wcr = Crater width, Hco = Cone height, Scr = Mean inner slope of crater, and Dcr = Crater depth.

indicated by the increase of magma flux (Table 4 and Fig. 9), and development of a complex plumbing system beneath Tianchi to form trachyte cones (0.61–0.25 Ma; Wei et al., 2007), successive basaltic intrusions may have been more readily captured by developing magma storage areas (Brenna et al., 2015b). This is supported by petrologic evidence for magma mixing/mingling, possibly associated with or triggering eruptive episodes (Fan et al., 2007b; Wei et al., 2007). A similar scenario occurs in the western part of the Trans-Mexican Volcanic Belt, Mexico, at Ceboruco and Tepetiltic (Petrone, 2010) and in Lamongan, Java, Indonesia (Carn and Pyle, 2001), where the magma that fed monogenetic volcanoes also fed and triggered polygenetic volcanoes. Evaluating the spatio-temporal development of dispersed monogenetic vents and their magma output rates can reflect the overall magma production in the area and provide insights into the development of polygenetic volcanoes.

The spatio-temporal distribution and geomorphological characteristics of monogenetic volcanoes can reflect different controls of magma propagation from source to surface. The alignments of the volcanoes in the LVF are approximately consistent with the local faults in three directions, and the elongate shape of the volcanic field is also consistent with one of the fault directions, which may indicate that the volcanic field is strongly affected by tectonic factors and crustal weaknesses. In contrast, the alignments of monogenetic volcanoes in the Tianchi area only coincide with faults in the NW-SE direction, and the shape of the volcanic area overall does not appear to be controlled by faults. This implies that lithospheric structural features and tectonics have a lesser impact on the Tianchi volcanic system compared to the LVF. Additionally, there is no clear radial vent alignment, and hence no obvious link with the central edifice plumbing system and locally induced stress regime (Acocella and Neri, 2009; Roman and Jaupart, 2014); this

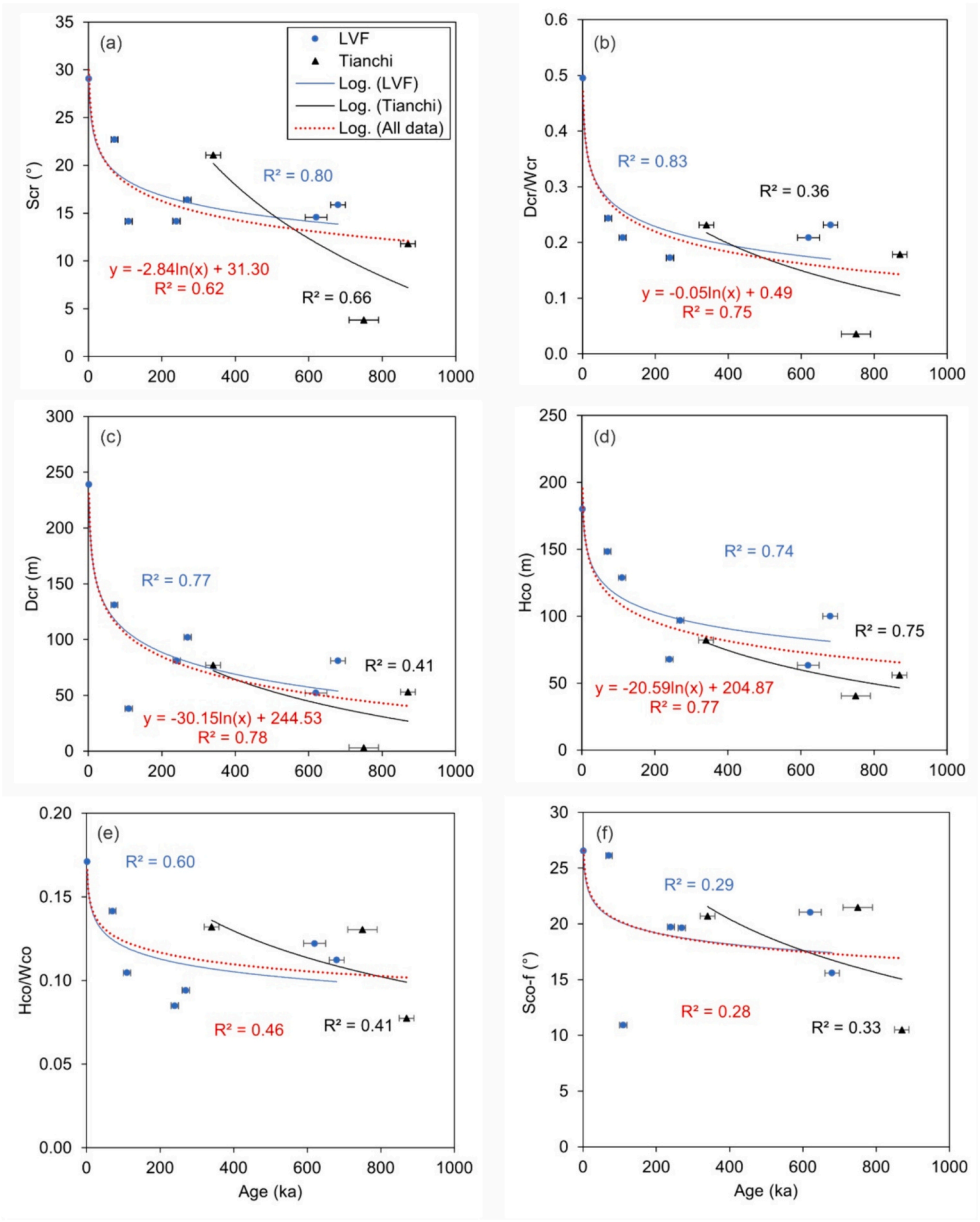

Fig. 7. Relationships between absolute age and morphometric parameters of scoria cones. (a) Age vs. Scr. (b) Age vs. Dcr/Wcr. (c) Age vs. Dcr. (d) Age vs. Hco. (e) Age vs. Hco/Wco. (f) Age vs. Sco-f. Wco = Cone base width, Wcr = Crater width, Hco = Cone height, Scr = Mean inner slope of crater, Dcr = Crater depth, and Sco-f = Mean flank slope of cone.

Table 3
Age group classification using Scr, Dcr, Hco and Dcr/Wcr parameters. Wcr = Crater width, Hco = Cone height, Scr = Mean inner slope of crater, and Dcr = Crater depth.

Parameter	Ancient	Old	Mature	Moderately mature	Young
Estimated age range	>870 ka	870–540 ka	540–340 ka	340–100 ka	≤100 ka
Scr[a]	<12.08°	12.08–13.43°	13.43–14.75°	14.75–18.22°	≥18.22°
Dcr/Wcr[b]	<0.15	0.15–0.18	0.18–0.20	0.20–0.26	≥0.26
Dcr[c]	<40 m	40–55 m	55–69 m	69–106 m	≥106 m
Hco[d]	<66 m	66–75 m	75–85 m	85–110 m	≥110 m

[a] . The threshold values for each relative age class are calculated using the formula in Fig. 7a.
[b] . The threshold values for each relative age class are calculated using the formula in Fig. 7b.
[c] . The threshold values for each relative age class are calculated using the formula in Fig. 7c.
[d] . The threshold values for each relative age class are calculated using the formula in Fig. 7d.

implies significant independence of the dispersed volcanoes from their coexisting polygenetic volcano (Yokoyama, 2015). Valentine and Perry (2007) proposed that the plumbing system of volcanoes with higher magma productivity (magmatically controlled) are less affected by pre-existing crustal structures. Moreover, according to the study of Morfulis et al. (2020) in the Southern Puna Plateau, Argentina, factors controlling

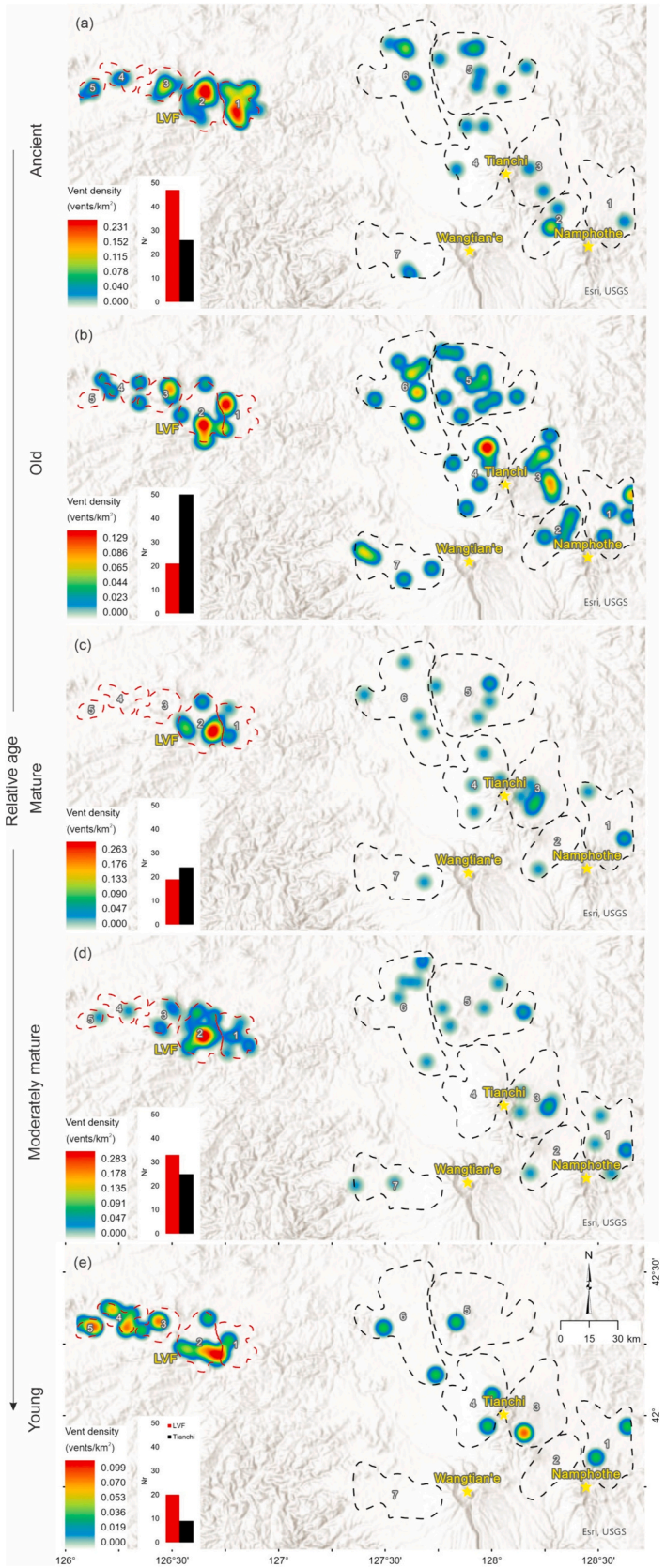

Fig. 8. Density maps and histograms of scoria cones with relative age classes (a) ancient, (b) old, (c) mature, (d) moderately mature and (e) young in the LVF and the Tianchi area. Other legends and base maps refer to Fig. 1.

Table 4
Output rate of monogenetic volcanic eruptions in the LVF and the Tianchi area.

Relative age class	Volcanic area	Cumulative scoria cone area (km^2)	Cumulative volume (km^3) *	Planimetric scoria cone output rate (km^2/kyr)	Volumetric volcanic output rate (km^3/kyr)
Old	LVF	13.265	4.948	0.040	0.015
	Tianchi	19.338	6.129	0.059	0.019
Mature	LVF	11.522	4.369	0.058	0.022
	Tianchi	11.938	3.787	0.060	0.019
Moderately mature	LVF	20.451	7.060	0.085	0.029
	Tianchi	17.655	7.039	0.074	0.029
Young	LVF	17.237	7.330	0.172	0.073
	Tianchi	6.585	3.007	0.066	0.030
Total	LVF	62.475	23.707	0.072	0.027
	Tianchi	55.517	19.962	0.064	0.023

* Volume is the total volume of scoria cones and associated lava flows. Ideal cone volume (Vco-eq.) is calculated according to Eq. 2 of Riedel et al. (2003), which assumes cones have reached the angle of repose and Hco/Wco and Wcr/Wco are the ideal values proposed by Porter (1972) and Wood (1980). Associated lava flow volume (Vla) is based on Eq. 5 (see Supplementary Data 1).

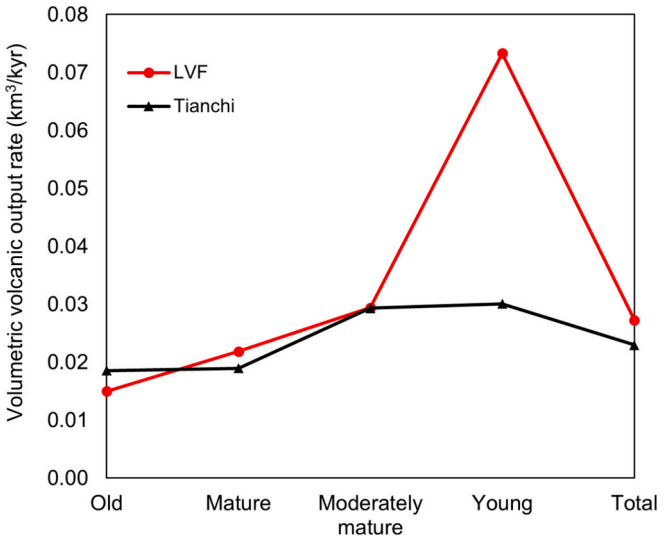

Fig. 9. Comparison of volumetric volcanic output rate in the two volcanic fields across age classes.

the distribution of vents in monogenetic volcanic fields can be divided into two overall types: control by magmatism, with more clustered distribution, and control by tectonism, with more random distribution. Following their framework, in the CVA, the magmatic evolution and eruptive system of the LVF are related to tectonic controls, whereas the development of the monogenetic volcanoes in the Tianchi area have a greater link to the magmatic source dynamics of the polygenetic volcano.

5.3. Transition between monogenetic volcanic field and polygenetic volcano

In the LVF, the number of scoria cones in the volcanic field is stable with markedly increased output rates from old to young (Figs. 8 and 9), indicating a corresponding increase in cone size. Fig. 10 shows that Wco tends to increase with decreasing age, both absolute and relative, in the LVF, suggesting the growth of larger cones with time. There are some other regions where this same trend has been identified. For instance, in the Jeju Island Volcanic Field, increased magma generation rates shifted volcanism from producing small-volume monogenetic volcanoes to accumulating large-volume volcanoes (Brenna et al., 2012, 2015a). Rangitoto is the youngest and largest monogenetic volcano in the Auckland Volcanic Field, and its formation is accompanied by an increase in magma output rate (Kereszturi et al., 2013b). In the Abu monogenetic volcanic group, Japan, although there was not a clear increment in individual volcano size, the overall output rates also increased over time (Kiyosugi et al., 2010). As these volcano characteristics are impacted by dynamic processes, such as tectonics and magma supply, they are not fixed for a given system, but may experience transitions from monogenetic to polygenetic activity (or vice versa). Quaternary volcanism in the Izu peninsula (Japan) was impacted by

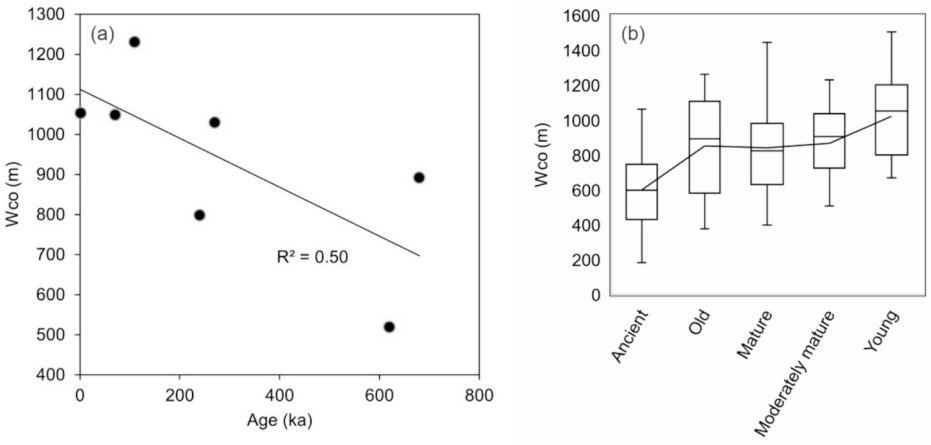

Fig. 10. (a) X-Y plot of age vs. Wco in the LVF for the seven cones having absolute ages. (b) Boxplot of Wco for the different relative age classes. Wco = Cone base width.

changes in stress field due to subduction dynamics, resulting in polygenetic activity building a stratovolcano that transitioned to dispersed small-volume monogenetic centres (Hasebe et al., 2001). In contrast, increasing complexity of mineral phases (olivine, clinopyroxene and plagioclase) in eruption products of the Wulanhada Volcanic Field (China) is interpreted as indicating the development of a crustal plumbing architecture favourable for the formation of a central polygenetic volcano (Luo et al., 2022). The coupling between magma supply and rate and tectonic activity has an impact on the resulting morphology. Ultimately, the transition of volcanic types in a single area can be evaluated by analysing spatial-temporal and geomorphological information of monogenetic volcanoes. An increase in Wco and/or more clustered vent distribution over time may represent the transition of factors controlling the volcanic activity and be a sign of the development of larger/polygenetic volcanoes. Therefore, detection of spatial-temporal pattern along with geomorphological characteristics of monogenetic volcanoes can hold key information to forecast and resolve evolution and associated volcanic hazards within volcanic fields.

6. Conclusions

The similarities and differences of monogenetic volcanoes in the LVF and the Tianchi area reveal different controlling factors within the CVA. Although their volcanic systems have similar magma source regions and output rate in the past 870 kyr, variations in the numbers of scoria cones in different age classes in the two volcanic fields suggest the influence of Tianchi volcano's magma system on the development of associated monogenetic volcanoes. Furthermore, the Tianchi area exhibits a more clustered vent distribution and an increased magma output rate, indicating monogenetic volcanoes in the Tianchi area are more magmatically controlled. Conversely, with more random vent distribution and better vent alignment, monogenetic volcanoes in the LVF are more likely influenced by tectonic factors such as faulting. Moreover, the continuous increase in magma output in the LVF suggests a potential risk of larger volcanoes occurring in the future.

The development and evolution of geomorphology, spatial-temporal information, and composition of monogenetic volcanoes are important research focuses for exploring and predicting volcanic eruption types and evaluating volcanic hazards. Comparing these characteristics between different monogenetic vent clusters in the same area can provide clues to the evolution and development of volcanic types in the area.

CRediT authorship contribution statement

Rong Zhang: Writing – original draft, Visualization, Resources, Methodology, Formal analysis, Conceptualization. **Marco Brenna:** Writing – review & editing, Supervision, Resources, Methodology, Conceptualization. **James D.L. White:** Writing – review & editing, Supervision, Methodology. **Gabor Kereszturi:** Writing – review & editing, Supervision, Methodology.

Declaration of competing interest

The authors declare that they have no known competing financial interests or personal relationships that could have appeared to influence the work reported in this paper.

Data availability

Data will be made available on request.

Acknowledgements

We thank the Doctoral Postgraduate Publishing Bursary provided by the University of Otago. We are grateful to Chuck Connor, Ian Schipper and Stephen Read for constructive discussion and feedback. Thanks to Bo Zhao for his help in data collection. We gratefully acknowledge Pablo Grosse and Martha Gabriela Gómez-Vasconcelos for their insightful comments and suggestions to improve the manuscript.

Appendix A. Supplementary data

Supplementary data to this article can be found online at https://doi.org/10.1016/j.jvolgeores.2024.108116.

References

Acocella, V., Neri, M., 2009. Dike propagation in volcanic edifices: overview and possible developments. Tectonophysics 471 (1–2), 67–77. https://doi.org/10.1016/j.tecto.2008.10.002.

Aguilera, M., Ureta, G., Grosse, P., Németh, K., Aguilera, F., Vilches, M., 2022. Geomorphological, morphometric, and spatial distribution analysis of the scoria cones in the Negros de Aras monogenetic volcanic field, northern Chile. J. Volcanol. Geotherm. Res. 422, 107458 https://doi.org/10.1016/j.jvolgeores.2021.107458.

Alaniz-Alvarez, S.A., Nieto-Samaniego, Á.F., Ferrari, L., 1998. Effect of strain rate in the distribution of monogenetic and polygenetic volcanism in the Transmexican volcanic belt. Geology 26 (7), 591–594. https://doi.org/10.1130/0091-7613(1998)026%3C0591:EOSRIT%3E2.3.CO;2.

Andreeva, O.A., Yarmolyuk, V.V., Andreeva, I.A., Ji, J.Q., Li, W.R., 2014. The composition and sources of magmas of Changbaishan Tianchi volcano (China-North Korea). In: Doklady Earth Sciences, 456. Pleiades Publishing, pp. 572–578. https://doi.org/10.1134/S1028334X14050213.

Bai, Z., Xu, D., Zhang, B., Zhang, T., Bu, J., 2006. Study on type and phase of Quaternary explosive volcanism in Longgang volcanic cluster. Acta Petrol. Sin. 22 (6), 1473-1480 500 (in Chinese).

Beggan, C., Hamilton, C.W., 2010. New image processing software for analyzing object size-frequency distributions, geometry, orientation, and spatial distribution. Comput. Geosci. 36 (4), 539–549. https://doi.org/10.1016/j.cageo.2009.09.003.

Bemis, K.G., Ferencz, M., 2017. Morphometric analysis of scoria cones: the potential for inferring process from shape. In: Németh, K., Carrasco-Núñez, G., Aranda-Gómez, J. J., Smith, I.E.M. (Eds.), Monogenetic Volcanism, Geological Society of London, Special Publications, 446, pp. 61–100. https://doi.org/10.1144/SP446.9.

Bemis, K., Walker, J., Borgia, A., Turrin, B., Neri, M., Swisher, C., 2011. The growth and erosion of cinder cones in Guatemala and El Salvador: models and statistics. J. Volcanol. Geotherm. Res. 201 (1–4), 39–52. https://doi.org/10.1016/j.jvolgeores.2010.11.007.

Brenna, M., Cronin, S.J., Smith, I.E., Sohn, Y.K., Maas, R., 2012. Spatio-temporal evolution of a dispersed magmatic system and its implications for volcano growth, Jeju Island Volcanic Field, Korea. Lithos 148, 337–352. https://doi.org/10.1016/j.lithos.2012.06.021.

Brenna, M., Cronin, S.J., Kereszturi, G., Sohn, Y.K., Smith, I.E., Wijbrans, J., 2015a. Intraplate volcanism influenced by distal subduction tectonics at Jeju Island, Republic of Korea. Bull. Volcanol. 77 https://doi.org/10.1007/s00445-014-0896-5.

Brenna, M., Nakada, S., Miura, D., Toshida, K., Ito, H., Hokanishi, N., Nakai, S.I., 2015b. A trachyte-syenite core within a basaltic nest: filtering of primitive injections by a multi-stage magma plumbing system (Oki-Dōzen, south-west Japan). Contrib. Mineral. Petrol. 170, 22. https://doi.org/10.1007/s00410-015-1181-0.

Bruno, B.C., Fagents, S.A., Hamilton, C.W., Burr, D.M., Baloga, S.M., 2006. Identification of volcanic rootless cones, ice mounds, and impact craters on Earth and Mars: using spatial distribution as a remote sensing tool. J. Geophys. Res. Planets 111 (E6). https://doi.org/10.1029/2005JE002510.

Cañón-Tapia, E., Walker, G.P., 2004. Global aspects of volcanism: the perspectives of "plate tectonics" and "volcanic systems". Earth Sci. Rev. 66(1–2), 163–182. doi: https://doi.org/10.1016/j.earscirev.2003.11.001.

Carn, S.A., 2000. The Lamongan volcanic field, East Java, Indonesia: physical volcanology, historic activity and hazards. J. Volcanol. Geotherm. 95 (1–4), 81–108. https://doi.org/10.1016/S0377-0273(99)00114-6.

Carn, S.A., Pyle, D.M., 2001. Petrology and geochemistry of the Lamongan volcanic field, East Java, Indonesia: Primitive Sunda arc magmas in an extensional tectonic setting? J. Petrol. 42 (9), 1643–1683. https://doi.org/10.1093/petrology/42.9.1643.

Cebriá, J.M., Martín-Escorza, C., López-Ruiz, J., Morán-Zenteno, D.J., Martiny, B.M., 2011. Numerical recognition of alignments in monogenetic volcanic areas: examples from the Michoacán-Guanajuato Volcanic Field in Mexico and Calatrava in Spain. J. Volcanol. Geotherm. Res. 201 (1–4), 73–82. https://doi.org/10.1016/j.jvolgeores.2010.07.016.

Chen, X., Wei, H., Yang, L., Chen, Z., 2017. Petrological and mineralogical characteristics of Tianchi volcano, Changbai Mountain: implications for crystallization differentiation and magma mixing. Acta Geosci. Sin. 38, 177–192 (in Chinese).

Cimarelli, C., Di Traglia, F., De Rita, D., Torrente, D.G., 2013. Space-time evolution of monogenetic volcanism in the mafic Garrotxa Volcanic Field (NE Iberian Peninsula). Bull. Volcanol. 75, 758. https://doi.org/10.1007/s00445-013-0758-6.

Clark, P.J., Evans, F.C., 1954. Distance to nearest neighbor as a measure of spatial relationships in populations. Ecology 35 (4), 445–453. https://doi.org/10.2307/1931034.

Condit, C.D., Connor, C.B., 1996. Recurrence rates of volcanism in basaltic volcanic fields: an example from the Springerville volcanic field, Arizona. Geol. Soc. Am. Bull. 108 (10), 1225–1241. https://doi.org/10.1130/0016-7606(1996)108%3C1225:RROVIB%3E2.3.CO;2.

Connor, C.B., Conway, F.M., 2000. Basaltic volcanic fields. In: Sigurdsson, H. (Ed.), Encyclopedia of Volcanoes. Academic Press, San Diego, pp. 331–343.
Fan, Q., Hooper, P.R., 1991. The Cenozoic basaltic rocks of eastern China: petrology and chemical composition. J. Petrol. 32 (4), 765–810. https://doi.org/10.1093/petrology/32.4.765.
Fan, Q., Sui, J., Liu, R., Wei, H., Li, N., 2000. Petrology and geochemistry of Jinlongdingzi active volcano-the most recent basaltic explosive volcano at Longgang. Chin. J. Geochem. 19 (4), 312–317.
Fan, Q., Sui, J., Liu, R., Wei, H., Li, D., Sun, Q., Li, N., 2002. Periods of Quarternary volcanic activity in Longgang area, Jilin province. Acta Petrol. Sin. 18, 495–500 (in Chinese).
Fan, Q., Sui, J., Wang, T., Li, N., Sun, Q., 2006. Eruption history and magma evolution of the trachybasalt in the Tianchi volcano, Changbaishan. Acta Petrol. Sin. 22 (6), 1449–1457 (in Chinese).
Fan, Q., Sui, J., Ni, L., Qian, S., 2007a. The magmatism and interactive eruption of the two magma chambers in the tianchi volcano, changbaishan. Bull. Mineral. Petrol. Geochem. 26 (4), 315–318 (In Chinese).
Fan, Q., Sui, J., Wang, T., Li, N., Sun, Q., 2007b. History of volcanic activity, magma evolution and eruptive mechanisms of the Changbai volcanic province. Geol. J. China Univ. 13 (2), 175–190 (In Chinese).
Favalli, M., Karátson, D., Mazzarini, F., Pareschi, M.T., Boschi, E., 2009. Morphometry of scoria cones located on a volcano flank: a case study from Mt. Etna (Italy), based on high-resolution LiDAR data. J. Volcanol. Geotherm. Res. 186 (3–4), 320–330. https://doi.org/10.1016/j.jvolgeores.2009.07.011.
Fedotov, S.A., 1981. Magma rates in feeding conduits of different volcanic centres. J. Volcanol. Geotherm. 9 (4), 379–394. https://doi.org/10.1016/0377-0273(81)90045-7.
Fornaciai, A., Favalli, M., Karátson, D., Tarquini, S., Boschi, E., 2012. Morphometry of scoria cones, and their relation to geodynamic setting: a DEM-based analysis. J. Volcanol. Geotherm. Res. 217, 56–72. https://doi.org/10.1016/j.jvolgeores.2011.12.012.
Grosse, P., Ramacciotti, M.L.O., Fochi, F.E., Guzmán, S., Orihashi, Y., Sumino, H., 2020. Geomorphology, morphometry, spatial distribution and ages of mafic monogenetic volcanoes of the Peinado and Incahuasi fields, southernmost Central Volcanic Zone of the Andes. J. Volcanol. Geotherm. Res. 401, 106966 https://doi.org/10.1016/j.jvolgeores.2020.106966.
Guilbaud, M.N., Siebe, C., Layer, P., Salinas, S., 2012. Reconstruction of the volcanic history of the Tacámbaro-Puruarán area (Michoacán, México) reveals high frequency of Holocene monogenetic eruptions. Bull. Volcanol. 74, 1187–1211. https://doi.org/10.1007/s00445-012-0594-0.
Haag, M.B., Baez, W.A., Sommer, C.A., Arnosio, J.M., Filipovich, R.E., 2019. Geomorphology and spatial distribution of monogenetic volcanoes in the southern Puna Plateau (NW Argentina). Geomorphology 342, 196–209. https://doi.org/10.1016/j.geomorph.2019.06.008.
Hasebe, N., Fukutani, A., Sudo, M., Tagami, T., 2001. Transition of eruptive style in an arc–arc collision zone: K–Ar dating of Quaternary monogenetic and polygenetic volcanoes in the Higashi-Izu region, Izu peninsula, Japan. Bull. Volcanol. 63, 377–386. https://doi.org/10.1007/s004450100158.
Hildreth, W., 1981. Gradients in silicic magma chambers: implications for lithospheric magmatism. J. Geophys. Res. Solid Earth 86 (B11), 10153–10192. https://doi.org/10.1029/JB086iB11p10153.
Hooper, D.M., Sheridan, M.F., 1998. Computer-simulation models of scoria cone degradation. J. Volcanol. Geotherm. Res. 83 (3–4), 241–267. https://doi.org/10.1016/S0377-0273(98)00031-6.
Ishizuka, O., Taylor, R.N., Geshi, N., Oikawa, T., Kawanabe, Y., Ogitsu, I., 2015. Progressive mixed-magma recharging of Izu-Oshima volcano, Japan: a guide to magma chamber volume. Earth Planet. Sci. Lett. 430, 19–29. https://doi.org/10.1016/j.epsl.2015.08.004.
Jin, B., Zhang, X., 1994. Researching Volcanic Geology in Mount Changbai. Northeast Korea Nation Education Press, Changchun, p. 223 (in Chinese).
Kereszturi, G., Németh, K., 2012a. Monogenetic basaltic volcanoes: Genetic classification, growth, geomorphology and degradation. In: Németh, K. (Ed.), Updates in Volcanology - New Advances in Understanding Volcanic Systems. InTech Open, Rijeka, Croatia, pp. 3–89. https://doi.org/10.5772/51387.
Kereszturi, G., Németh, K., 2012b. Structural and morphometric irregularities of eroded Pliocene scoria cones at the Bakony-Balaton Highland Volcanic Field, Hungary. Geomorphology 136 (1), 45–58. https://doi.org/10.1016/j.geomorph.2011.08.005.
Kereszturi, G., Jordan, G., Németh, K., Dóniz-Páez, J.F., 2012. Syn-eruptive morphometric variability of monogenetic scoria cones. Bull. Volcanol. 74, 2171–2185. https://doi.org/10.1007/s00445-012-0658-1.
Kereszturi, G., Geyer, A., Martí, J., Németh, K., Dóniz-Páez, F.J., 2013a. Evaluation of morphometry-based dating of monogenetic volcanoes—a case study from Bandas del Sur, Tenerife (Canary Islands). Bull. Volcanol. 75, 734. https://doi.org/10.1007/s00445-013-0734-1.
Kereszturi, G., Németh, K., Cronin, S.J., Agustín-Flores, J., Smith, I.E., Lindsay, J., 2013b. A model for calculating eruptive volumes for monogenetic volcanoes—implication for the Quaternary Auckland Volcanic Field, New Zealand. J. Volcanol. Geotherm. Res. 266, 16–33. https://doi.org/10.1016/j.jvolgeores.2013.09.003.
Kereszturi, G., Németh, K., Cronin, S.J., Procter, J., Agustín-Flores, J., 2014. Influences on the variability of eruption sequences and style transitions in the Auckland Volcanic Field, New Zealand. J. Volcanol. Geotherm. Res. 286, 101–115. https://doi.org/10.1016/j.jvolgeores.2014.09.002.
Kervyn, M., Ernst, G.G.J., Carracedo, J.C., Jacobs, P., 2012. Geomorphometric variability of "monogenetic" volcanic cones: evidence from Mauna Kea, Lanzarote and experimental cones. Geomorphology 136 (1), 59–75. https://doi.org/10.1016/j.geomorph.2011.04.009.
Kimura, J.I., Sakuyama, T., Miyazaki, T., Vaglarov, B.S., Fukao, Y., Stern, R.J., 2018. Plume-stagnant slab-lithosphere interactions: origin of the late Cenozoic intra-plate basalts on the East Eurasia margin. Lithos 300, 227–249. https://doi.org/10.1016/j.lithos.2017.12.003.
Kiyosugi, K., Connor, C.B., Zhao, D., Connor, L.J., Tanaka, K., 2010. Relationships between volcano distribution, crustal structure, and P-wave tomography: an example from the Abu Monogenetic Volcano Group, SW Japan. Bull. Volcanol. 72, 331–340. https://doi.org/10.1007/s00445-009-0316-4.
Kuritani, T., Kimura, J.I., Miyamoto, T., Wei, H., Shimano, T., Maeno, F., Jin, X., Taniguchi, H., 2009. Intraplate magmatism related to deceleration of upwelling asthenospheric mantle: Implications from the Changbaishan shield basalts, northeast China. Lithos 112 (3–4), 247–258. https://doi.org/10.1016/j.lithos.2009.02.007.
Kuritani, T., Xia, Q.K., Kimura, J.I., Liu, J., Shimizu, K., Ushikubo, T., Zhao, D., Nakagawa, M., Yoshimura, S., 2019. Buoyant hydrous mantle plume from the mantle transition zone. Sci. Rep. 9 (1), 6549. https://doi.org/10.1038/s41598-019-43103-y.
Le Corvec, N., Spörli, K.B., Rowland, J., Lindsay, J., 2013. Spatial distribution and alignments of volcanic centers: clues to the formation of monogenetic volcanic fields. Earth Sci. Rev. 124, 96–114. https://doi.org/10.1016/j.earscirev.2013.05.005.
Lei, M., Guo, Z., Sun, Y., Zhang, M., Zhang, L., Ma, L., 2019. Geochemical constraints on the origin of late Cenozoic basalts in the Mt. Changbai volcanic field, NE China: evidence for crustal recycling. Int. Geol. Rev. 62 (17), 2125–2145. https://doi.org/10.1080/00206814.2019.1686660.
Leonard, G.S., Calvert, A.T., Hopkins, J.L., Wilson, C.J., Smid, E.R., Lindsay, J.M., Champion, D.E., 2017. High-precision 40Ar/39Ar dating of Quaternary basalts from Auckland Volcanic Field, New Zealand, with implications for eruption rates and paleomagnetic correlations. J. Volcanol. Geotherm. Res. 343, 60–74. https://doi.org/10.1016/j.jvolgeores.2017.05.033.
Li, M., Xu, Z., Ventura, G., Pan, X., Han, D., Gu, G., Yan, D., Pan, B., Feng, J., 2021. Geochronology and petrogenesis of Early Pleistocene Dikes in the Changbai Mountain Volcanic Field (NE China) based on geochemistry and Sr-Nd-Pb-Hf isotopic compositions. Front. Earth Sci. 9, 729905 https://doi.org/10.3389/feart.2021.729905.
Liu, J., 1988. The cenozoic volcanic episodes in Northeast China. Acta Petrol. Sin. 1 (1) (In Chinese).
Liu, Y., 1990. The structural characteristics of the Longgang volcano group in Jilin. Reg. Geol. China 2, 157–185 (In Chinese).
Liu, J., 1999. Volcanoes of China. Science Press of China, Beijing (In Chinese).
Liu, R., 2000. Active Volcanoes of China. Earthquake Press, Beijing (In Chinese).
Liu, X., Xiang, T., Wang, X., 1989. Episodes of Cenozoic volcanism in the Changbai mountains area. Jilin Geol. 1, 30–41 (In Chinese).
Liu, R., Chou, S., Cai, L., Wei, H., Yang, Q., Xian, Z., Bo, G., Zhong, J., 1997. Study on the age of the last great eruption of changbaishan tianchi volcano and its significance. Sci. China Ser. D Earth Sci. 27 (5), 438–441 (In Chinese).
Liu, J., Chu, G., Han, J., Rioual, P., Jiao, W., Wang, K., 2009. Volcanic eruptions in the Longgang volcanic field, northeastern China, during the past 15,000 years. J. Asian Earth Sci. 34 (5), 645–654. https://doi.org/10.1016/j.jseaes.2008.09.005.
Luo, D., Reichow, M.K., Hou, T., Santosh, M., Zhang, Z., Wang, M., Qin, J., Yang, D., Pan, R., Wang, X., Holtz, F., 2022. A snapshot of the transition from monogenetic volcanoes to composite volcanoes: case study on the Wulanhada Volcanic Field (northern China). Eur. J. Mineral. 34 (5), 469–491. https://doi.org/10.5194/ejm-34-469-2022.
Lutz, T.M., 1986. An analysis of the orientations of large-scale crustal structures: a statistical approach based on areal distributions of pointlike features. J. Geophys. Res. Solid Earth 91 (B1), 421–434. https://doi.org/10.1029/JB091iB01p00421.
Martin, U., Németh, K., 2006. How Strombolian is a "Strombolian" scoria cone? Some irregularities in scoria cone architecture from the Transmexican Volcanic Belt, near Volcán Ceboruco (Mexico) and Al Haruj (Libya). J. Volcanol. Geotherm. Res. 155 (1–2), 104–118. https://doi.org/10.1016/j.jvolgeores.2006.02.012.
Mazzarini, F., 2007. Vent distribution and crustal thickness in stretched continental crust: the case of the Afar Depression (Ethiopia). Geosphere 3 (3), 152–162. https://doi.org/10.1130/GES00070.1.
Morfulis, M., Báez, W., Retamoso, S., Bardelli, L., Filipovich, R., Sommer, C.A., 2020. Quantitative spatial distribution analysis of mafic monogenic volcanism in the southern Puna, Argentina: implications for magma production rates and structural control during its ascent. J. S. Am. Earth Sci. 104, 102852 https://doi.org/10.1016/j.jsames.2020.102852.
Murcia, H., Németh, K., 2020. Effusive monogenetic volcanism. In: Updates in Volcanology-Transdisciplinary Nature of Volcano Science. Intech Open. https://doi.org/10.5772/intechopen.94387.
Németh, K., Kereszturi, G., 2015. Monogenetic volcanism: personal views and discussion. Int. J. Earth Sci. 104 (8), 2131–2146. https://doi.org/10.1007/s00531-015-1243-6.
Ou, X., Fu, Q., 1984. The relationship between the Longgang volcanic group and tectonic activity. Jiling Geol. 1, 76–81 (In Chinese).
Paguican, E.M., Grosse, P., Fabbro, G.N., Kervyn, M., 2021. Morphometric classification and spatial distribution of Philippine volcanoes. J. Volcanol. Geotherm. Res. 418, 107251 https://doi.org/10.1016/j.jvolgeores.2021.107251.
Petrone, C.M., 2010. Relationship between monogenetic magmatism and stratovolcanoes in western Mexico: the role of low-pressure magmatic processes. Lithos 119 (3–4), 585–606. https://doi.org/10.1016/j.lithos.2010.08.012.
Porter, S.C., 1972. Distribution, morphology, and size frequency of cinder cones on Mauna Kea volcano, Hawaii. Geol. Soc. Am. Bull. 83 (12), 3607–3612. https://doi.org/10.1130/0016-7606(1972)83[3607:DMASFO]2.0.CO;2.
Qian, C., Cui, T., Tang, Z., Jiang, B., Zhang, C., Qin, T., Lu, L., Chen, H., Wu, T., 2016. Stage division and genesis discussion of basaltic volcanism during the cone-forming

stage of Tianchi volcano in Changbaishan region. Geol. China 43, 1963–1976 (in Chinese).
Riedel, C., Ernst, G.G.J., Riley, M., 2003. Controls on the growth and geometry of pyroclastic constructs. J. Volcanol. Geotherm. Res. 127 (1–2), 121–152. https://doi.org/10.1016/S0377-0273(03)00196-3.
Roman, A., Jaupart, C., 2014. The impact of a volcanic edifice on intrusive and eruptive activity. Earth Planet. Sci. Lett. 408, 1–8. https://doi.org/10.1016/j.epsl.2014.09.016.
Runge, M.G., Bebbington, M.S., Cronin, S.J., Lindsay, J.M., Kenedi, C.L., Moufti, M.R.H., 2014. Vents to events: determining an eruption event record from volcanic vent structures for the Harrat Rahat, Saudi Arabia. Bull. Volcanol. 76, 804. https://doi.org/10.1007/s00445-014-0804-z.
Schmidt, C., Laag, C., Whitehead, M., Profe, J., Aka, F.T., Hasegawa, T., Kereszturi, G., 2022. The complexities of assessing volcanic hazards along the Cameroon Volcanic Line using spatial distribution of monogenetic volcanoes. J. Volcanol. Geotherm. Res. 427, 107558 https://doi.org/10.1016/j.jvolgeores.2022.107558.
Sui, J., Fan, Q., Cao, J., 1999. A preliminary study of eruption features and petrochemistry of volcanic rocks from the Longgang volcanoes. Geol. Rev. 45 (Suppl), 319–324 (In Chinese).
Sun, Y., Guo, Z., Fortin, D., 2021. Carbon dioxide emission from monogenetic volcanoes in the Mt. Changbai volcanic field, NE China. Int. Geol. Rev. 63 (14), 1803–1820. https://doi.org/10.1080/00206814.2020.1802782.
Takada, A., 1994. The influence of regional stress and magmatic input on styles of monogenetic and polygenetic volcanism. J. Geophys. Res. Solid Earth 99 (B7), 13563–13573. https://doi.org/10.1029/94JB00494.
Takaku, J., Tadono, T., Tsutsui, K., 2014. Generation of high resolution global DSM from ALOS PRISM. Int. Arch. Photogramm. Remote. Sens. Spat. Inf. Sci. XL-4, 243–248. https://doi.org/10.5194/isprsarchives-XL-4-243-2014.
Tang, Y., Obayashi, M., Niu, F., Grand, S.P., Chen, Y.J., Kawakatsu, H., Tanaka, S., Ning, J., Ni, J.F., 2014. Changbaishan volcanism in Northeast China linked to subduction-induced mantle upwelling. Nat. Geosci. 7 (6), 470–475. https://doi.org/10.1038/ngeo2166.
Thomson, B.J., Lang, N.P., 2016. Volcanic edifice alignment detection software in MATLAB: Test data and preliminary results for shield fields on Venus. Comput. Geosci. 93, 1–11. https://doi.org/10.1016/j.cageo.2016.04.012.
Valentine, G.A., Connor, C.B., 2015. Basaltic volcanic fields. In: Sigurdsson, H. (Ed.), The Encyclopedia of Volcanoes. Academic Press, pp. 423–439.
Valentine, G.A., Perry, F.V., 2007. Tectonically controlled, time-predictable basaltic volcanism from a lithospheric mantle source (central Basin and Range Province, USA). Earth Planet. Sci. Lett. 261 (1–2), 201–216. https://doi.org/10.1016/j.epsl.2007.06.029.
van den Hove, J., Grose, L., Betts, P.G., Ailleres, L., Van Otterloo, J., Cas, R.A., 2017. Spatial analysis of an intra-plate basaltic volcanic field in a compressional tectonic setting: South-eastern Australia. J. Volcanol. Geotherm. Res. 335, 35–53. https://doi.org/10.1016/j.jvolgeores.2017.02.001.
Wang, Y., Li, C., Wei, H., Shan, X., 2003. Late Pliocene–recent tectonic setting for the Tianchi volcanic zone, Changbai Mountains, Northeast China. J. Asian Earth Sci. 21 (10), 1159–1170. https://doi.org/10.1016/S1367-9120(03)00019-1.
Wei, H., Yang, Q., 1998. The geology of the Tianchi Volcano, Changbaishan. In: Liu, R., Wei, H., Li, J. (Eds.), Latest Eruptions from the Tianchi Volcano, Changbaishan. Science Press, Beijing (In Chinese).
Wei, H., Liu, R., Yang, Q., 1998a. Physical volcanology study on Tianchi Volcano. In: Liu, R., Wei, H., Li, J. (Eds.), Latest Eruptions from Tianchi Volcano, Changbaishan. Science Press, Beijing (In Chinese).
Wei, H., Song, S., Yang, Q., Liu, X., 1998b. The recent erupted materials from Tianchi volcano, Changbaishan. In: Liu, R., Wei, H., Li, J. (Eds.), Latest Eruptions from Tianchi Volcano, Changbaishan. Science Press, Beijing (In Chinese).
Wei, H., Liu, R., Fan, Q., Jin, B., Liu, X., Zhang, C., 1999. Monogenetic volcanism in Longgang volcano clusters. Geol. Rev. 45 (3252), 331.
Wei, H., Wang, Y., Jin, J., Gao, L., Yun, S.H., Jin, B., 2007. Timescale and evolution of the intracontinental Tianchi volcanic shield and ignimbrite-forming eruption, Changbaishan, Northeast China. Lithos 96 (1–2), 315–324. https://doi.org/10.1016/j.lithos.2006.10.004.
Wei, H., Liu, G., Gill, J., 2013. Review of eruptive activity at Tianchi volcano, Changbaishan, Northeast China: implications for possible future eruptions. Bull. Volcanol. 75, 706. https://doi.org/10.1007/s00445-013-0706-5.
Wollschlaeger, D., 2022. Package 'shotGroups'. https://cran.r-project.org/web/packages/shotGroups/shotGroups.pdf (Accessed 05 November 2022).
Wood, C.A., 1979. Monogenetic volcanoes of the terrestrial planets. Proc. Lunar Planet. Sci. Conf. 10th, pp. 2815–2840.
Wood, C.A., 1980. Morphometric evolution of cinder cones. J. Volcanol. Geotherm. Res. 7 (3–4), 387–413. https://doi.org/10.1016/0377-0273(80)90040-2.
Xie, Y., Liu, X., Xiang, T., 1993. The Researches on Cenozoic Volcanoes and Volcanic Rocks in the Middle District of Northeast China, 237. Northeast Normal University Press, Changchun (in Chinese).
Xu, Q., Liu, J., He, H., Zhang, Y., 2019. Nature and evolution of the lithospheric mantle revealed by water contents and He-Ar isotopes of peridotite xenoliths from Changbaishan and Longgang basalts in Northeast China. Sci. Bull. 64 (18), 1325–1335. https://doi.org/10.1016/j.scib.2019.07.006.
Yang, Q., Jenkins, S.F., Lerner, G.A., Li, W., Suzuki, T., McLean, D., Derkachev, A.N., Utkin, I.V., Wei, H., Xu, J., Pan, B., 2021. The Millennium eruption of Changbaishan Tianchi volcano is VEI 6, not 7. Bull. Volcanol. 83, 74. https://doi.org/10.1007/s00445-021-01487-8.
Yokoyama, I., 2015. Eruption patterns of parasitic volcanoes. Ann. Geophys. 58 (3), S0327. https://doi.org/10.4401/ag-6557.
Yu, F., Han, S., Ma, Z., Xie, R., 2005. Uranium series chronology of the late Pleistocene basalt from the Longgang volcanoes, Jilin Province. Acta Geol. Sin. Engl. Ed. 79 (2), 211–214. https://doi.org/10.1111/j.1755-6724.2005.tb00883.x.
Zhang, M., Guo, Z., Cheng, Z., Zhang, L., Liu, J., 2015. Late Cenozoic intraplate volcanism in Changbai volcanic field, on the border of China and North Korea: Insights into deep subduction of the Pacific slab and intraplate volcanism. J. Geol. Soc. Lond. 172 (5), 648–663. https://doi.org/10.1144/jgs2014-080.
Zhang, M., Guo, Z., Liu, J., Liu, G., Zhang, L., Lei, M., Zhao, W., Ma, L., Sepe, V., Ventura, G., 2018. The intraplate Changbaishan volcanic field (China/North Korea): a review on eruptive history, magma genesis, geodynamic significance, recent dynamics and potential hazards. Earth Sci. Rev. 187, 19–52. https://doi.org/10.1016/j.earscirev.2018.07.011.
Zhang, B., Lei, J., Yuan, X., Zhang, G., He, J., Xu, Q., 2020. Detailed Moho variations under Northeast China inferred from receiver function analyses and their tectonic implications. Phys. Earth Planet. Inter. 300, 106448 https://doi.org/10.1016/j.pepi.2020.106448.
Zhang, R., Kereszturi, G., Brenna, M., Ahn, U.S., 2022. Sensitivity assessment of morphometric parameters of monogenetic volcanic landforms with global free DEMs. Geomorphology 108408. https://doi.org/10.1016/j.geomorph.2022.108408.
Zhang, R., Brenna, M., Kereszturi, G., 2023. Monogenetic scoria cone and associated lava flow volume estimates and their controlling factors. J. Volcanol. Geotherm. Res. 107872 https://doi.org/10.1016/j.jvolgeores.2023.107872.
Zhao, D., Tian, Y., Lei, J., Liu, L., Zheng, S., 2009. Seismic image and origin of the Changbai intraplate volcano in East Asia: role of big mantle wedge above the stagnant Pacific slab. Phys. Earth Planet. Inter. 173 (3–4), 197–206. https://doi.org/10.1016/j.pepi.2008.11.009.
Zhao, B., Xu, D., Bai, Z., Chen, Z., 2021. Volcanism in the Longgang volcanic field of NE China: insights from eruption history, volcano types and geochemical characteristics. Geol. Soc. Lond. Spec. Publ. 510 (1), 27–39. https://doi.org/10.1144/SP510-2020-60.
Zhao, B., Xu, D., Bai, Z., Chen, Z., 2022. Hydro-volcanism in the Longgang Volcanic Field, Northeast China: insights from topography, stratigraphy, granulometry and microtexture of Xidadianzi Maar Volcano. Minerals 12 (9), 1113. https://doi.org/10.3390/min12091113.
Zou, H., Fan, Q., Yao, Y., 2008. U-Th systematics of dispersed young volcanoes in NE China: asthenosphere upwelling caused by piling up and upward thickening of stagnant Pacific slab. Chem. Geol. 255 (1–2), 134–142. https://doi.org/10.1016/j.chemgeo.2008.06.022.